An expanded record of Early Cambrian carbon cycling from the Anti-Atlas Margin, Morocco

Adam C. Maloof, Daniel P. Schrag, James L. Crowley, and Samuel A. Bowring

Abstract: We present a $\delta^{13}C$ record from the Anti-Atlas mountains of Morocco and place it in the context of a detailed regional tectonostratigraphy. We place the litho- and chemostratigraphic record in a temporal framework using precision U–Pb zircon geochronology of ashes interbedded with the same carbonate units that provide $\delta^{13}C$ data. The variations in $\delta^{13}C$ of carbonate occur on a wide range of time scales, suggesting that different mechanisms are involved, including non-steady state release of isotopically depleted carbon reservoirs on short (<100 000 years) time scales and changes in nutrient recycling and organic carbon burial on longer (≥1 Ma) time scales. Through a correlation with more fossiliferous, albeit condensed, sections in Siberia, we examine the pattern of cyclic $\delta^{13}C$ variation in the context of the reappearance and diversification of skeletonized metazoa during the Early Cambrian.

Résumé : Nous présentons des données $\delta^{13}C$ des montagnes de l'Anti-Atlas du Maroc et nous les examinons dans le contexte d'une tectonostratigraphie régionale détaillée. Nous insérons les données lithostratigraphiques et chimiostratigraphiques dans un cadre temporel en utilisant une géochronologie U–Pb de précision sur des zircons provenant de cendres interlitées avec les mêmes unités de carbonates qui ont fourni les données $\delta^{13}C$. Les $\delta^{13}C$ des carbonates varient sur une grande plage d'échelles de temps, suggérant que différents mécanismes sont en jeu, incluant le relâchement en régime variable de réservoirs de carbone épuisés sur une courte échelle de temps (<100 000 ans) et des changements dans le recyclage des nutriments et de l'enfouissement du carbone organique selon des échelles de temps plus longues (≥1 Ma). En corrélation avec des sections plus fossilifères mais condensées provenant de Sibérie, nous examinons le patron des variations cycliques des données $\delta^{13}C$ dans le contexte d'une résurgence et de la diversification de métazoaires squelettisés au cours du Cambrien précoce.

[Traduit par la Rédaction]

Introduction

Three billion years of Earth history without large animal fossils came to a close ~575 Ma with the appearance of soft-bodied Ediacaran fauna (Narbonne and Gehling 2003, Narbonne 1998, Fedonkin 1990, Cloud and Glaessner 1982). Between 555 and 542 Ma, organisms very gradually began to scratch deeper and more complicated traces into sandstones (Martin et al. 2000, Gehling et al. 2001, Jensen et al. 2000) while a low-diversity suite of calcified metazoa colonized microbial bioherms (Wood et al. 2002, Hoffmann and Mountjoy 2001, Grotzinger et al. 2000). At 542 Ma, a global carbon isotope excursion to –6‰ (Amthor et al. 2003, Corsetti and Hagadorn 2000 Bartley et al. 1998, Kaufman et al. 1997, Knoll et al. 1995*a*, Narbonne et al. 1994) marked the abrupt last-appearance of most, if not all, Ediacara (Jensen et al. 1998, Crimes et al. 1995, Conway Morris 1993, Hagadorn et al. 2000, Crimes and McIlroy 1999, Brasier 1995, Seilacher 1984), as well as the prominent calcified metazoa *Cloudina* and *Namacalathus* (Grotzinger et al. 2000, Watters and Grotzinger 2001, Grant 1990, Germs 1972).

Between 542 and ~530 Ma (Nemakit-Daldyn), burrowers gradually began to dig deeper in sediment (e.g., Crimes 1987) and calcifying organisms reappeared slowly, their hardparts being preserved as small shelly fossils in the phosphatizating environments of the Early Cambrian (Porter 2004). The Nemakit-Daldyn (ND) – Tommotian (Tm) boundary (525.5 Ma, this paper) corresponded to (1) an abrupt increase in diversity and abundance of calcifying organisms, both in the form of reef-building Archaeocyatha (Debrenne 1991, Zhuravlev 1986) and small shelly fauna (Khomentovsky and Karlova 1993, Rowland et al. 1998), and (2) the first appearance of significant vertical burrowing (e.g., *Skolithos* and *Diplocraterion*) in siliciclastic sediments (Bottjer et al. 2000, Orr et al. 2003, Droser et al. 1999, Droser et al. 2002). Carbon-isotopic data from Siberia suggest that the ND–Tm boundary is associated with a peak in $\delta^{13}C$ as high as 5‰ (Magaritz et al. 1986, Knoll et al. 1995*a*). However, the presence of a sub-Tommotian unconformity and relatively slow sediment accumulation rates in Siberia (Knoll et al. 1995*b*, Pelechaty et al. 1996, Kouchinsky et al. 2001) has left a condensed picture of faunal radiation and $\delta^{13}C$ variability across the ND–Tm boundary.

In this contribution, we present detailed chemostratigraphies from the Anti-Atlas mountains of Morocco, collected at 0.2–1.5 m sampling intervals through 2.5 km of nearly continuous

Received 21 September 2004. Accepted 26 May 2005. Published on the NRC Research Press Web site at http://cjes.nrc.ca/ on 14 February 2006.

Paper handled by Associate Editor G.R. Dix

Adam C. Maloof[1,2] and Daniel P. Schrag. Department of Earth and Planetary Sciences, Harvard University, 20 Oxford Street, Cambridge, MA 02138, USA.
James L. Crowley and Samuel A. Bowring. Department of Earth, Atmospheric and Planetary Sciences, Massachusetts Institute of Technology, 77 Massachusetts Ave., Cambridge, MA 02139, USA.

[1]Present Address: Department of Earth, Atmospheric and Planetary Sciences, Massachusetts Institute of Technology, 77 Massachusetts Ave., Cambridge, MA 02139, USA.
[2]Corresponding author (e-mail: maloofa@mit.edu).

 doi: 10.1139/E05-062

carbonate sediment spanning the Early Cambrian. We calibrate the peak of the Tommotian $\delta^{13}C$ high with a U–Pb zircon age of an ash fall tuff in the same section and develop a high resolution record of $\delta^{13}C$ variability through the Early Cambrian. Finally, we show that the $\delta^{13}C$ behavior of the Nemakit-Daldyn is very similar to that of the Early Triassic (Payne et al. 2004), and that fluctuations in the fractional burial of organic carbon following era-ending mass extinctions (Magaritz 1989) may have a common cause (or consequence?).

Tectonostratigraphic setting

During the Hercynian orogeny, the northern edge of the West African Craton (WAC) was warped into the broad northeast-southwest-trending anticlinorium that forms the Anti-Atlas mountains. The Anti-Atlas mountains are bounded to the south by Mesozoic cover of the cratonic Tindouf basin, and to the north by the South Atlas Fault (SAF, Fig. 1), an ancient structure active most recently as a Cenozoic thrust fault (Gomez et al. 2000, Frizon de Lamotte et al. 2000, Beauchamp et al. 1999). In the Anti-Atlas, irregular buckle folding of the contact between Precambrian basement and Paleozoic sediments stranded erosional remnants of basement culminations (boutonnières or inliers) in a sea of Paleozoic sedimentary cover (Cartig et al. 2004, Faik et al. 2001, Leblanc and Lancelot 1972). The inliers record a Precambrian history of the northern margin of the WAC and accreted Pan-African terranes, while the rims of inliers tell the tale of Earth's transition from the Proterozoic to Paleozoic eras (Michard 1976).

Pre-600 Ma evolution of the WAC's northern margin

South of the Anti-Atlas major fault (AAMF, Fig. 1), basement inliers are composed of 2070 Ma metasediments (Walsh et al. 2002) intruded by 2050–2032 Ma granitoids (Walsh et al. 2002, Thomas et al. 2002, Roger et al. 2001, Hassenforder et al. 2001, Mortaji et al. 2000, Aït Malek et al. 1998) similar in age to the Birimian crust that makes up most of the WAC (Boher et al. 1992). Taghdout Group (Fig. 1) basalts, quartzites, and stromatolitic–oolitic carbonates rest unconformably on the Paleoproterozoic basement and represent a platformal succession deposited on the northern margin of the WAC (Bouougri and Saquaque 2000, El Aouli et al. 2001, Thomas et al. 2002, Hafid et al. 2001). North of the AAMF in the eastern High Atlas, virtually no traces of Eburnean basement are present and the oldest intact rocks are thick piles of basalts and turbidites of the Saghro Group (Fig. 1). The Saghro Group has been interpreted as a distal-slope equivalent of the Taghdout Group, deposited between the WAC to the south and an island arc (Thomas et al. 2002, Bouougri 2003) or slivers of rifted Eburnean crust (Fekkak et al. 2000, Fekkak et al. 2002, Ouguir et al. 1996, Fekkak et al. 2001), such as Cadomia (Samson and D'Lemos 1998), to the north. Igneous zircons from the Iriri migmatite (Siroua) provide a crystallization age for northern arc rocks later accreted during the Pan-African collision and have an age of 743±13 Ma (Thomas et al. 2002). A 762^{+1}_{-2} Ma leucogranite dyke intruded contemporaneously with gabbros of the Tasriwine ophiolite (Siroua inlier) provides a crystallization age for some of the oceanic crust later obducted during Pan-African Orogeny (Samson et al. 2004).

The Taghdout and Saghro groups were deformed during the Pan-African orogeny, when closure of a marginal sea led to the southward obduction and sinistral translation of ophiolitic mélanges (Hurley et al. 1974, Leblanc 1976, El Boukhari et al. 1992, Thomas et al. 2002) and northern terranes along the AAMF. In the El Graara inlier, the 650 Ma Aït Ahmane quartz diorite (unpublished U–Pb zircon age of S.D. Samson, cited in (Hefferan et al. 2000) intrudes the deformed Bou Azzer ophiolite and provides a minimum age on Pan-African accretionary tectonics. Metamorphic overgrowths on zircons in the Iriri migmatite associated with the obducted ophiolite complex in Siroua inlier date Pan-African deformation at 663 ± 13 Ma.

Post-600 Ma rifting of the WAC's northern margin

Fanglomerates and coarse siliciclastics of the Tiddiline Group (Fig. 1) fill fault-bounded basins that rest unconformably on folded Pan-African assemblages and post-Pan-African granitic intrusions. Clasts of the 579.4±1.2 Ma Bleida granodiorite (Inglis et al. 2004, Ducrot 1979) are abundant in conglomerates and place a maximum age on the onset of Tiddiline Group deposition. The Tiddiline Group has been interpreted either as syn-collisional molasse (Saquaque et al. 1989, Hefferan et al. 1992) or rift-related fill (Piqué et al. 1999, Soulaïmani et al. 2001, Piqué 2003, Soulaïmani et al. 2003), but the latter interpretation is favored given the ~80 Ma gap between Pan-African orgenesis and Tiddiline extension.

The Ouarzazate Group (Fig. 1) reflects the onset of rift volcanism and covers the pre- and syn-Pan-African basement with a 0–2000 m thick blanket of felsic lavas, ignimbrites, and volcaniclastics. Distinctive volcanic centers intruded by high-level granites characterize the Ouarzazate Group and, in concert with rift-related normal faulting, lead to abundant lateral facies changes and internal angular discordances (Thomas et al. 2002). Although much of the Ouarzazate Group was deposited subaerially, lacustrine deposits are common around the flanks of volcanic centers and in the cores of collapsed calderas.

Ouarzazate Group volcanics and associated high-level granites fill a narrow age range between 577 and 560 Ma (Thomas et al. 2002, Walsh et al. 2002, Mifdal and Peucat 1985, Aït Malek et al. 1998). Furthermore, felsic lavas and ash flow tuffs from the uppermost Ouarzazate Group have remarkably similar ages across the Anti-Atlas, suggesting near synchronous termination of rift volcanism at ~560 Ma: 560.0±2.1 Ma for the Houssi El Gah rhyolite at Bas Drâa (Maloof 2004), 564.6±3.2 Ma for the Igherm tuff (Maloof 2004), 562.89 ± 0.49 Ma for the Minount rhyodacite northwest of Timjich (this paper), 563 ± 5 Ma for the Tiouine ignimbrites northeast of Siroua (Mifdal and Peucat 1985), and 565 ± 7 Ma for the Upper Ouarzazate Group ignimbrite in Tagrara de Tata inlier (Walsh et al. 2002).

The Early Cambrian passive margin

With the cessation of volcanism and onset of thermal subsidence, the rifted Pan-African margin was flooded. The first marine transgression across the rifted Pan-African margin marks the base of the Taroudant Group, which itself is composed of the Adoudou and Lie de Vin formations.

Adoudou Formation

Traditionally, the Adoudou Formation was divided into a basal unit dubbed the Série de Base, and an upper unit called

Fig. 1. Tectonostratigraphic map of the pre-Middle Cambrian Anti-Atlas mountains, Morocco (Saadi et al. 1985).

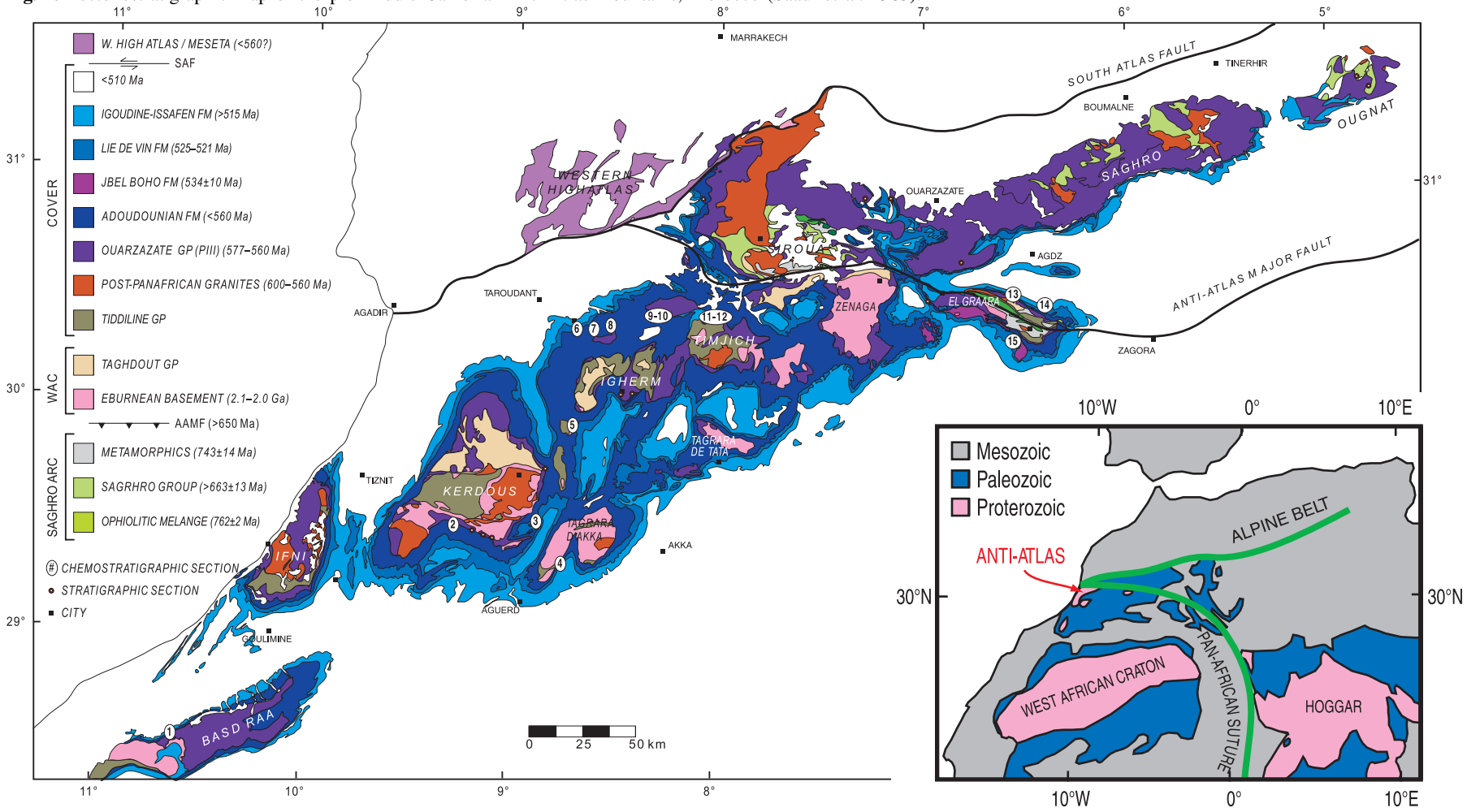

Fig. 2. Chemostratigraphy of the Anti-Atlas mountains, west. The sedimentology is vastly oversimplified and plotted lithofacies (see Fig. 3) are only meant to represent the lithologies that dominate a particular unit. $\delta^{13}C$ data in MS-6 (Tiout) are from Tucker (1986) and Magaritz et al. (1991).

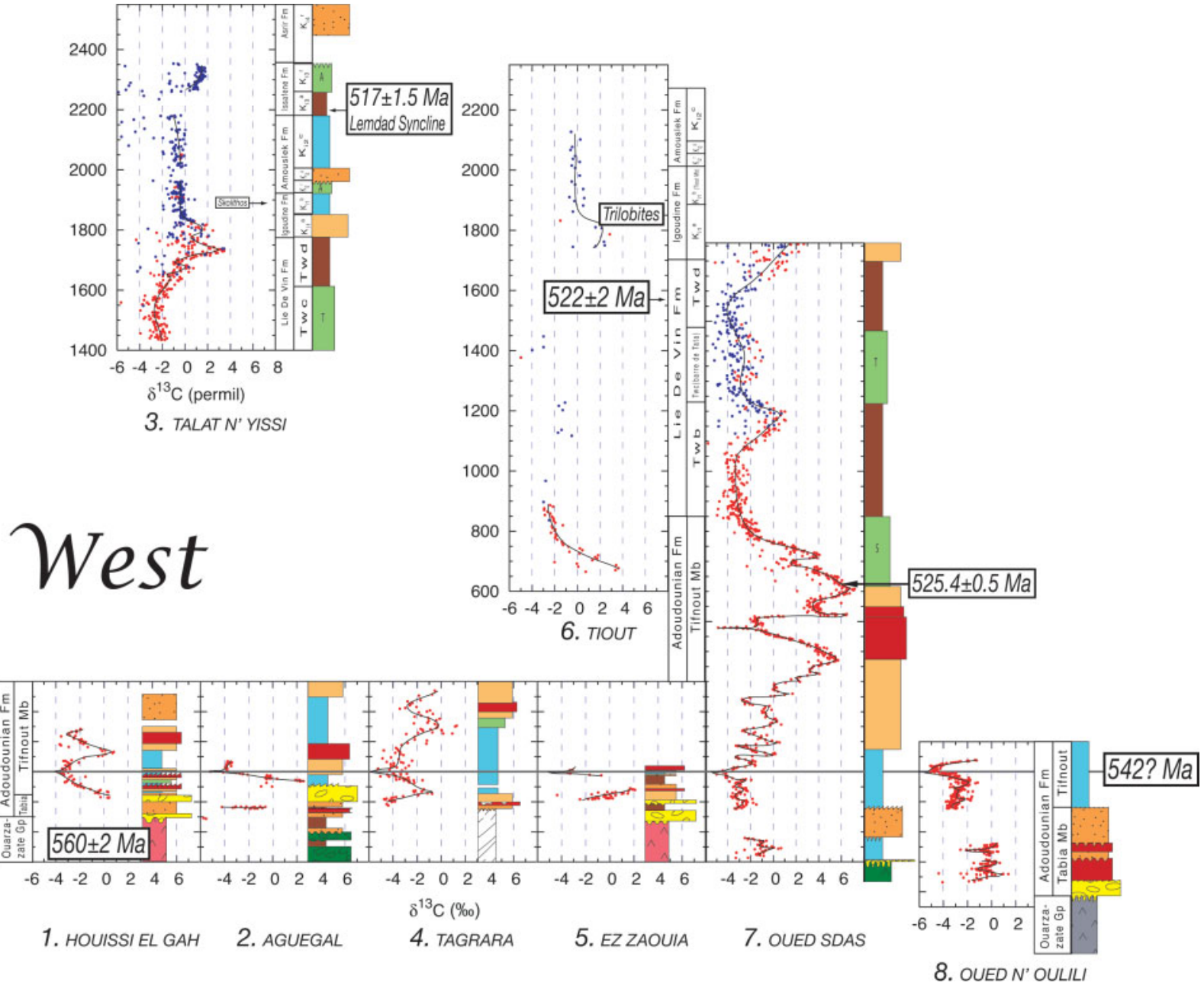

the Calcaires Supérieurs. Here, we elevate these two units to member status. We define the Tabia Member (a town in the Oulili river where the Tabia Member is developed best, MS-8, Fig. 2) as the 0–250 m of peritidal carbonates, evaporites, mudcracked siltstones, fluvial sandstones, and coarse siliciclastic debris that was deposited in a series of linked half grabens with steep bounding normal faults (Destombes et al. 1985, Benziane et al. 1983, Azizi Samir et al. 1990, Chbani et al. 1999, Algouti et al. 2000, Algouti et al. 2001, Benssaou and Hamoumi 1999*c*, Benssaou and Hamoumi 1999*b*, Benssaou and Hamoumi 1999*a*, Benssaou and Hamoumi 2001, Benssaou and Hamoumi 2003). Tidally dominated fine-siliciclastics of the uppermost Tabia Member often contain discoid structures of unknown affinity that superficially resemble Ediacaran fauna, such as *Aspidella* (MS-2, MS-7, Igherm (Houzay 1979), and Tioune).

The Tifnout Member of the Adoudou Formation (named after a town in the Sdas river where the Tifnout Member is thickest, MS-7, Fig. 2) reflects the end of abundant regional block faulting and the beginning of a thermal subsidence-dominated regime. Peritidal dolostones blanket virtually the entire Anti-Atlas, thinning to the east and south, from 1000 m thick at Oued Sdas (MS-7), to $<$ 300 m thick in the El Graara (MS-13-15) and Bas Drâa (MS-1) inliers, to nonexistent in Saghro and Ougnat inliers (Fig. 1, (Geyer and Landing 1995, Geyer 1989, Destombes et al. 1985)). Where the Tifnout Member is relatively thin, dolostones are arranged in metre-scale, shallowing-upwards parasequences that typically begin with siltstones and marls, are followed by wavy-laminated micrites and grainstones, and are capped by microbialaminites (sometimes stromatolites) often showing signs of subaerial exposure, such as pseudomorphs after gypsum, teepees (Kendall and Warren 1987), desiccation cracks, and karstic, ferruginized and (or) silicified parasequence boundaries. Where the Tifnout Member is thick, individual parasequences are thicker and evidence of subaerial exposure is much less common. The rheological instability inherent in a thick stack of finely interbedded siltstones and dolostones made the Tifnout Member susceptible to slump folding and brecciation on various scales (Buggisch and Heinitz 1984).

In the El Graara inlier (Fig. 1, 3), andesitic and trachytic flows and autobreccias are interbedded with the Tifnout Member. The Jbel Boho syenite plug, which crosscuts most of the lavas, was dated at 534 $\pm$ 10 Ma (Ducrot and Lancelot 1977) and provides a minimum age for at least the lower Tifnout Member. In the southwest corner of El Graara inlier, (Buggisch and Flügel 1988) report calcified algae *Kundatia composita* KORDE in stromatolites of the lower Tifnout Member consistent with an Early Cambrian age for the dolostones. Unfortunately, the lack of suitable coarse siliciclastic facies is likely part of the reason why the Tifnout Member is barren of diagnostic trace fossils that might constrain its age more precisely.

Lie de Vin Formation

The Lie de Vin Formation reflects the stratigraphic response of seaward tilting or flexure of the Anti-Atlas margin. Similar to the Adoudou Formation, the Lie de Vin Formation thins to the east and south from 950 m at Tiout (MS-6) to $<$15 m in El Graara (MS-13, MS-14, MS-15) and Bas Drâa (MS-1). Landward, the Lie de Vin Formation represents a significant sea-level regression, with erosional beveling of underlying units in the far east and the progradation of the fluvial Tikirt Member sandstone westward and northward across the basin (Fig. 3*b*). Seaward, the Lie de Vin Formation actually records an increase in relative sea level and a switch from peritidal dolostone sedimentation to sublittoral deposition of purple argillite – biohermal limestone couplets (Monninger 1979, Destombes et al. 1985). The argillites reflect an increase in the siliclastic sediment reaching the basin and are likely basinward equivalents of the Tikirt Member sandstone.

Out-of-phase landward versus basinward relative sea-level patterns are common on margins that developed through rifting of warm, thickened continental lithosphere (Kooi and Cloetingh 1992). Extensional thinning of lithosphere usually leads to preferential necking at a level where the lithosphere is strong (Braun and Beaumont 1989*b*, Braun and Beaumont 1989*a*, Zuber and Parmentier 1986)). Strength profiles of warm, thickened lithosphere suggest that this zone of maximum strength would occur at shallow to moderate intracrustal depths of 15–20 km (Braun and Beaumont 1989*a*). Rifted continental margins that underwent necking at 15–20 km depth commonly undergo a transition from upward-flexed rift margins in their youth to downwarped rift shoulders after sufficient cooling of the lithosphere and sediment accumulation increases the flexural load on the basin (Kooi et al. 1992). Dense dolostones of the Tifnout Member would have accumulated during the early phases of thermal subsidence with upwarped rift shoulders (Fig. 3*b*, middle panel). The out-of-phase relative sea-level pattern of the Lie de Vin Formation would reflect the transition to downwarped rift flanks and a seaward tilting of the margin. This transition to a downward-flexure mode also is associated with a major increase in sediment accumulation rate (Fig. 8). It is possible that the voluminous crustal melting that characterizes the Ouarzazate Group led to important basaltic underplating of zones of thinned crust. Eventual eclogitization of the underplated basalts could have added an additional flexural load to the basin, accelerating sediment accumulation rates, and assisting the transition to the downwarped rift flanks of the Lie de Vin Formation.

Cyclic alternations of burgundy colored argillite and biohermal carbonates in the Lie de Vin Formation have captured the imagination of every worker that has visited Tiout (e.g., Monninger 1979, Latham and Riding 1990, Geyer and Landing 1995). On a metre scale, as is so with the Adoudou Formation, these lithological alternations form autocylclic, shoaling-upwards parasequences. In the case of the Lie de Vin Formation, complete parasequences consist of a flooding surface, followed by interbedded argillite and wavy carbonate laminite, followed by stromatolite and (or) thrombolite bioherms that pass laterally into grainstones, followed by the next flooding surface. Many parasequences are incomplete and appear as argillite–thrombolite couplets. We counted 150 parasequences in 880 m of the Lie de Vin Formation at Oued Sdas (MS-7). Monninger (1979) found $\sim$180 parasequences in 940 m at Tiout (MS-6). Climatic, tectonic, and eustatic signals of various characteristic time scales modulate the total thickness of parasequences, as well as the relative proportion of biohermal carbonate to argillite in individual parasequences, to yield a pattern of cyclothems (10–20 cycles) and supercycles (20–100 cycles). Whether these cycles represent stationary periodic signals or Poisson processes is always a point of contention (Wilkinson et al. 1997, Wilkinson et al. 1999, Bailey 1998, Yang et al. 1995, Kominz and Bond 1990, Goldhammer et

Fig. 3. (A) Chemostratigraphy of the Anti-Atlas mountains, East. The sedimentology is vastly oversimplified and plotted lithofacies are only meant to represent the lithologies that dominate a particular unit; (B) Schematic evolution of the post-Pan-African margin. Top panel: Tabia Member of the Adoudou Formation is deposited in a series of link half grabens bounded by normal faults. Middle panel: Tifnout Mb of the Adoudou Fm is deposited on a broad, thermally subsiding passive margin. Bottom panel: The Lie de Vin Formation, deposited as the margin, is tilted seaward, leading to landward regression (Tikirt Member) and seaward deepening.

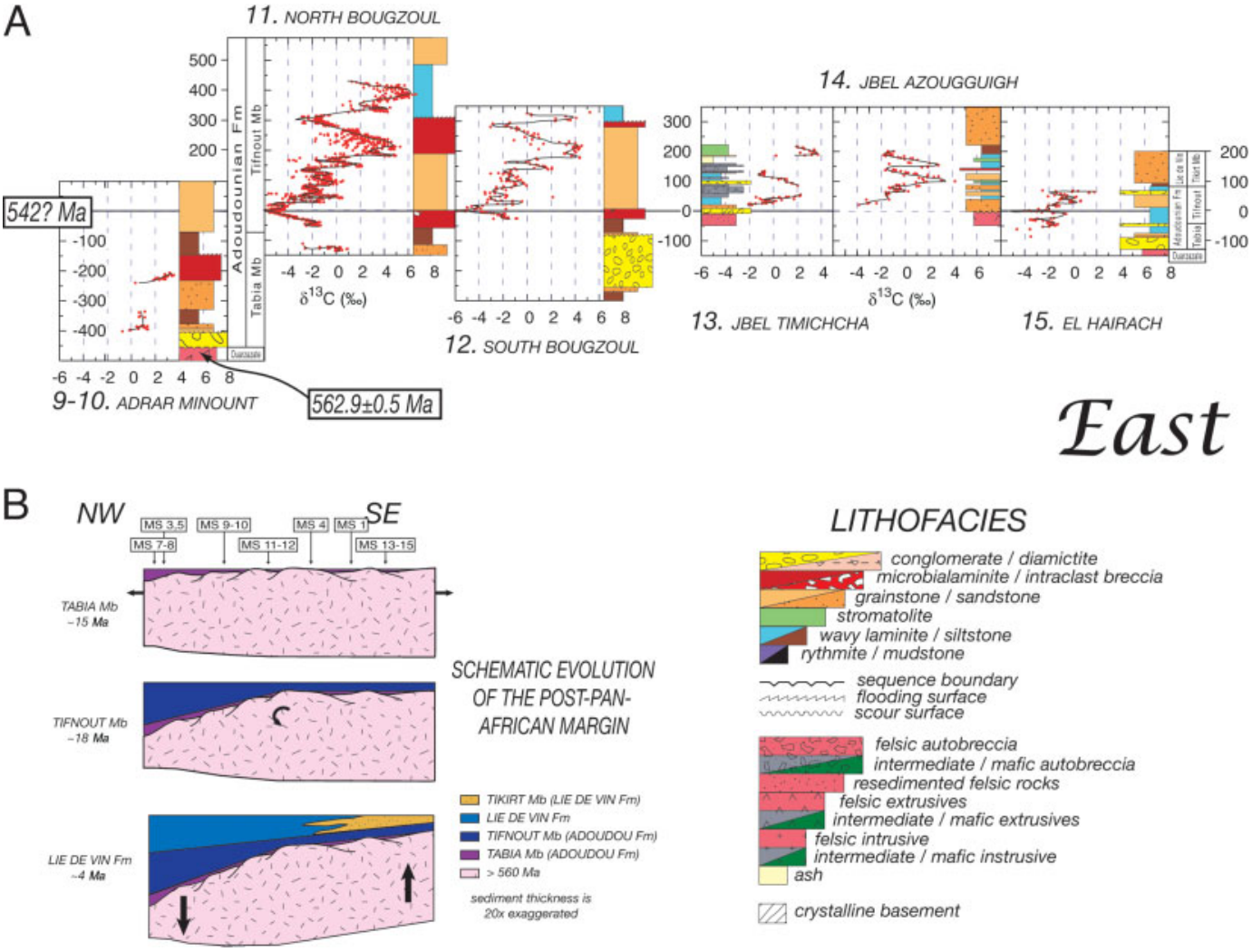

al. 1987, Grotzinger 1986, Goodwin and Anderson 1985). Sediment accumulation rates on shallow carbonate ramps, such as the Early Cambrian of the Anti-Atlas, vary stochastically on short time scales and preclude reliable spectral analysis. However, on a 10^6 year-time-scale, sediment accumulation rates may average out sufficiently to permit the recognition of coherent signals. As shown in Fig. 4, the proportion of biohermal carbonate relative to argillite oscillates with a characteristic period of ~1.2 Ma. In contrast, the presence of five to six parasequence-thickness cycles suggest a period of ~750 ka, although the signal is not obviously periodic or correlated with biohermal abundace and $\delta^{13}C$. At Tiout, Monninger (1979) also found three "limestone-content" and five parasequence-thickness supercycles over the same interval, suggesting that these features are reproducible at least within the same basin.

An ash from the upper Lie de Vin Formation at Tiout (MS-6, Fig. 1, 2) has an age of 522.4±2.0 Ma (Landing et al. 1998, Compston et al. 1992). Carbon isotope data from Tiout (Tucker 1986) and Oued Sdas (Magaritz et al. 1991) have been coupled with magnetostratigraphic data from Tiout (Kirschvink et al. 1991) to draw correlations with the chemostratigraphy of Siberia and are not inconsistent with a Tommotian age for the Lie de Vin Formation. The limestone bioherms are stromatolitic or thrombolitic and commonly contain calcified algae, such as *Tarthinia*, *Renalcis*, and *Kordephyton* (Latham and Riding 1990, Bertrand-Safarti 1981). Although indistinct trace fossils are common, dolostone grainstones often appear weakly bioturbated, occurrences of the vertical burrow *Diplocraterion* have been reported from Tiout (Latham and Riding 1990), and horizontal traces of *Diplichnites*-type, which are thought to be arthropod tracks, are found in the upper Tikirt Member of the Siroua area (Geyer and Landing 1995), diagnostic fossils

Fig. 4. Relative proportion of biohermal carbonate (stromatolites and thrombolites) to mud (light blue) and parasequence thickness (green) plotted against parasequence number. Also shown is $\delta^{13}C$ (red) versus stratigraphic height. The black curve highlights the low order variability common to both biohermal carbonate percentage and $\delta^{13}C$. Approximate ages at endpoints are based on linear interpolation between U–Pb zircon dates from ashes.

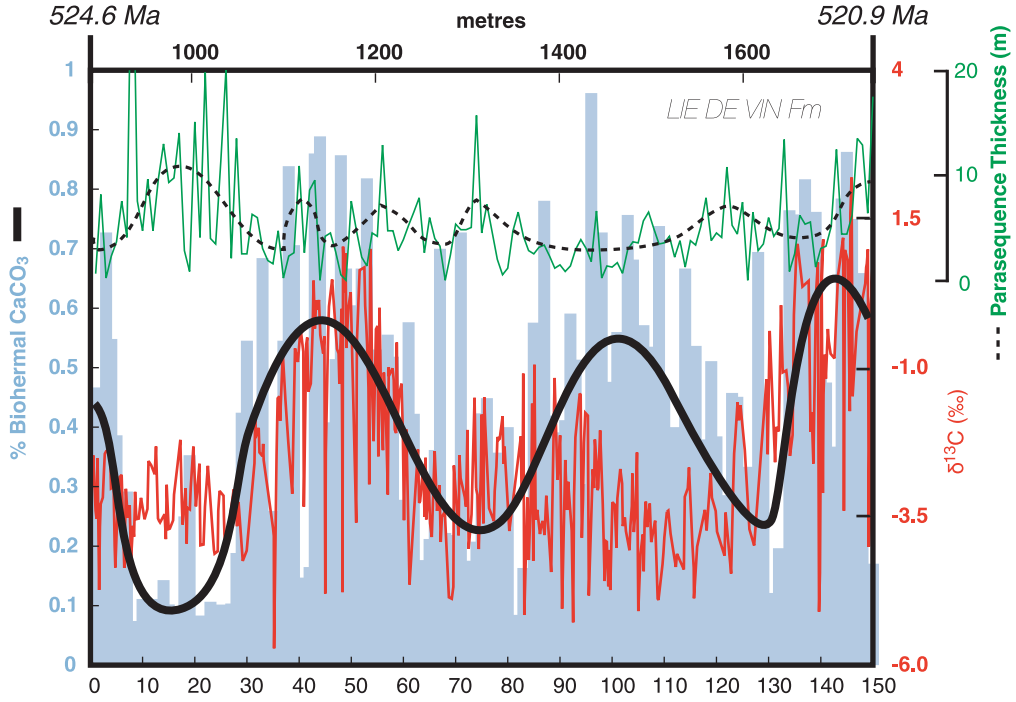

amenable to interregional correlation have not been described.

Tata Group

The Tata Group represents the remainder of Early Cambrian strata above the Taroudant Group and includes the Igoudine, Amouslek, and Issafene formations, and their correlatives (Geyer and Landing 1995). In general, the base of the Tata Group represents a transition to more energetic marine conditions than those found in the Lie de Vin Formation (Destombes et al. 1985, Geyer 1989, Hupé 1953). Shoaling-upwards parasequences are common, beginning with green or grey shales, followed by black limestone wavy laminates, and capped by trilobite-hash packstones, cross-bedded ooilitic grainstones, or archaeocyathan–algal bioherms. Subaerial exposure, desiccation, and vadose gypsum precipitation affected the tops of some parasequences, although exposure surfaces are not nearly as common as they are in the Adoudou Formation. As with all Early Cambrian strata in the Anti-Atlas, siliciclastic sediments become more important to the east and south.

The Igoudine Formation contains the oldest known skeletal fossils from Morocco (Choubert and Hupé 1953, Choubert et al. 1975, Boudda et al. 1979). Trilobites of the *Eofallotaspis* Zone first appear in the Tiout Member (upper Igoudine Formation) (Geyer and Landing 1995), often within a few metres of the first *Erismacoscinus fasciolus – Reteoscinus minutus* Zone archeocyathans (Hupé 1953, Debrenne and Debrenne 1978, Debrenne and Debrenne 1995), brachiopods, and chancelloriids. Trilobites in the uppermost Tiout Member transition into the *Fallotaspis tazemmourtensis* Zone. The Amouslek Formation is characterized by *Choubertella* and *Daguinaspis* zone trilobites (Geyer and Landing 1995) and *Erismacoscinus maro-canus* Zone archeocyathids (Debrenne and Debrenne 1995). Trilobites of the *Antatlasia hollardi*, *Antatlasia gutta-pluviae*, and *Sectigena* Zone appear sequentially in the Issafen Formation, coincident with the transition to the *Polystillicidocyathus – Halysicyathus* archeocyathid Zone. An ash bed from the equivalent to the lower Issafen Formation in the Lemdad syncline of the High Atlas is dated at 517 ± 1.5 Ma (Landing et al. 1998) and is consistent with an Atdabanian–Botomian age for the Tata Group.

Chemostratigraphy

$\delta^{13}C$ methods

Carbonate samples were collected while measuring stratigraphic sections. Clean dolostones and limestones without siliciclastic components or secondary veining or cleavage were targeted. Samples were slabbed and polished perpendicular to bedding and ~5 mg of powder was micro-drilled from individual laminations for isotopic analysis. $\delta^{13}C$ and $\delta^{18}O$ were measured simultaneously on a VG Optima dual inlet mass spectrometer attached to a VG isocarb preparation device in the Harvard University Laboratory for Geochemical Oceanography, Cambridge, Massachusetts. Approximately 1 mg of the carbonate powder was reacted in a common H_3PO_4 bath at 90° for 8–10 min. Evolved CO_2 was purified and collected cryogenically and then analyzed against an in-house reference gas. The analytical uncertainty (1σ) of this measurement was $<\pm 0.1‰$. Samples were calibrated to VPDB (Vienna Pee Dee Belemnite) using six measurements of the Cararra Marble standard for each run of 54 samples. Memory effect associated with the common acid bath system was minimized by increasing the reaction time for

dolomite samples and monitoring the measured values of standards. Examination of the variation in standards after each run showed that the error due to memory effect was always <0.2‰.

δ^{13}C results

Chemostratigraphic plots for 15 measured sections across the Anti-Atlas mountains are presented in Figs. 2 and 3 and are summarized in Fig. 5. δ^{13}C of the Tabia Member is difficult to correlate between sections, but, in general, varies between −4‰ and 0‰. The lower Tifnout Member shows near uniformity across the basin, descending rapidly from −2‰ at the base to a low of −6‰. δ^{13}C then increases in an oscillatory fashion from −6‰ to a high of +7‰ in the upper Tifnout Member. In the uppermost Tifnout Member (600 m, Fig. 5), δ^{13}C crashes again to −3‰ and stays between −3.5‰ and 0.5‰ for most of the Lie de Vin Formation. δ^{13}C rises to a peak of 3.5‰ in the uppermost Lie de Vin and lower Igoudine formations and then stabilizes at −0.5‰ for the remainder of the Tata Group.

Superimposed on these broad trends is a hierarchy of δ^{13}C oscillations with different characteristic periods and amplitudes. High-frequency signals with periods $\leq 10^5$ year and amplitudes of 1‰–3‰ are present as semi-coherent signals in the scatter from 1400–1700 m (Fig. 5) and as very well-defined excursions, such as the negative spike at 480 m (Figs. 5, 6). Even higher order variability of <1‰ amplitude may be present (e.g., Fig. 6), but our sampling density was often too coarse to determine whether or not this variability reflects coherent oscillations. However, we can state with certainty that there is no simple correlation between facies and high-frequency δ^{13}C variability, either within parasequences or over the stratigraphic section as a whole. Moderate frequency oscillations with periods of $\sim 10^6$ year and amplitudes of 2‰–4‰ characterize the entire time series (Fig. 5), and in the Lie de Vin Formation, are apparent in two different lithofacies parameters (Fig. 4). Lower order, 4–7 Ma period, 8‰–11‰ amplitude signals are particularly obvious in the middle–upper Adoudou Formation between 300 and 800 m.

Oxygen isotopes are plotted in Fig. 5. In the Taroudant Group, few trends are discernible in the smear of very high- frequency variability and (or) noise with a mean value of –6‰ to –7‰. A few hundred metres below the base of the Tata Group, mean δ^{18}O descends to –14‰ and remains highly depleted until the uppermost Early Cambrian. δ^{13}C versus δ^{18}O cross plots show no statistically significant covariation of the two isotopic systems (not plotted).

Because fluids responsible for diagenetic recrystallization of carbonates may replace completely the original population of oxygen atoms in the rock, most workers discard δ^{18}O data from carbonates that have undergone significant fluid–rock interactions (Brand and Veizer 1981, Banner and Hanson 1990, Pearson et al. 2001). Furthermore, oxygen isotopic studies of Phanerozoic ophiolite complexes suggest that the δ^{18}O composition of seawater is buffered against long-term changes by hydrothermal alteration of basalt around mid-ocean ridges (Muehlenbachs and Clayton 1976, Muehlenbachs 1998, Gregory and Taylor 1981, Holmden and Muehlenbachs 1993). Nevertheless, it is worth documenting that the basic δ^{18}O signal observed in Morocco is similar to trends produced in other Neoproterozoic–Paleozoic data sets around the world. Such data sets indicate an evolving oxygen-isotopic composition of seawater, with values of –4‰ to –10‰ in the Neoproterozoic (Jacobsen and Kaufman 1999) dropping to a nadir in the late Early Cambrian to Late Cambrian of –10‰ to –14‰, and then rising through the Phanerozoic to modern values of 0‰ (Veizer et al. 1999).

U–Pb zircon geochronology

U–Pb methods

Zircon was extracted from samples by standard crushing, Wilfley table, heavy-liquid, and magnetic separation. Analyzed grains were selected from the least magnetic fraction based on the absence of cracks, inclusions, and surface contamination. To minimize Pb-loss, zircon was subjected to standard physical air abrasion (Krogh 1982) or a version of the chemical abrasion technique (Mattinson 2003). Grains that underwent air abrasion were ultrasonicated in 30% HNO_3 for 1 h, fluxed in 30% HNO_3 at ∼80 °C for 1 h, and rinsed in ultrapure acetone and H_2O before being loaded into 300 μL Teflon FEP microcapsules and spiked with a mixed ^{233}U–^{235}U–^{205}Pb tracer. Zircon was dissolved in ∼120 μL 29 mol/L HF with ∼25 μL 30% HNO_3 at ∼210 °C for 48 h, dried to fluorides, and then re-dissolved in 6 mol/L HCl at ∼180 °C overnight. Grains that underwent chemical abrasion were placed in a muffle furnace at 900±20 °C for ∼60 h in quartz beakers before being transferred to 300 μL Teflon FEP microcapsules and leached in ∼120 μL 29 mol/L HF + ∼25 μL 30% HNO_3 for 12–14 h at ∼180 °C. Grains were rinsed in ultrapure H_2O, fluxed on a hotplate at ∼80 °C for 1 h in 6 mol/L HCl, ultrasonicated for 1 h, placed back on the hotplate for an additional 30 min, and rinsed in ultrapure acetone and H_2O. Grains were then loaded back into microcapsules, which were rinsed with ultrapure H_2O and fluxed on a hotplate with 30% HNO_3 or 6 mol/L HCl, and then spiked and fully dissolved using the procedure just described. U and Pb were separated using an HCl based anion-exchange chromatographic procedure (Krogh 1973).

U and Pb isotopic measurements were performed on a VG Sector-54 multi-collector thermal-ionization mass spectrometer at MIT, Cambridge, Massachusetts. Pb and U were loaded together on a single Re filament in a silica-gel–phosphoric acid mixture (Gerstenberger and Haase 1997). Pb was measured by peak-hopping on a single Daly detector and U isotopic measurements were made in static Faraday mode. Mass fractionation on the Daly detector was determined to be 0.25 ± 0.04%/amu (atomic mass unit) over a wide temperature range based on analysis of the NBS-981 common Pb standard and spiked aliquots of NBS-983. U mass fractionation was calculated in real-time using a double spike. All common Pb was attributed to procedural blank. A sensitivity test shows that the composition of the common Pb has no effect on the calculated dates. U blanks were <0.1 pg. Data reduction, age calculation, and the generation of concordia plots were done using the algorithms of (Ludwig 1980), and (or) using the statistical reduction and plotting program ISOPLOT (Ludwig 1991).

In the past few years, it has become evident that zircons that yield high-precision statistically equivalent data sets often have slight age discordance (^{207}Pb/^{206}Pb dates are a minimum of 0.2% older than the U–Pb dates), likely due to imprecision in one or both of the U decay constants (Mattinson 2000). In many previous studies of lower Paleozoic zircon plagued with Pb loss that is inferred to have occurred in recent times, ^{207}Pb/^{206}Pb

Fig. 5. Summary of $\delta^{13}C$ and $\delta^{18}O$ versus stratigraphic height for MS-3, MS-4, MS-6 (data from Tucker (1986) and Magaritz et al. (1991)), MS-7, MS-8, and MS-10 to MS-12 (see Figs. 1–3 for measured section locations and stratigraphic detail). Ages along the right edge of the graph are U–Pb zircon ages from Morocco, except for the 542.0 date which is based on correlation of the −6‰ $\delta^{13}C$ nadir with the Precambrian–Cambrian boundary carbon isotope excursion observed worldwide (Amthor et al. 2003, Grotzinger et al. 1995, Knoll and Carroll 1999, Kimura and Watanabe 2001). Age transitions highlighted in yellow are based on global correlation of $\delta^{13}C$ and fossil zonation.

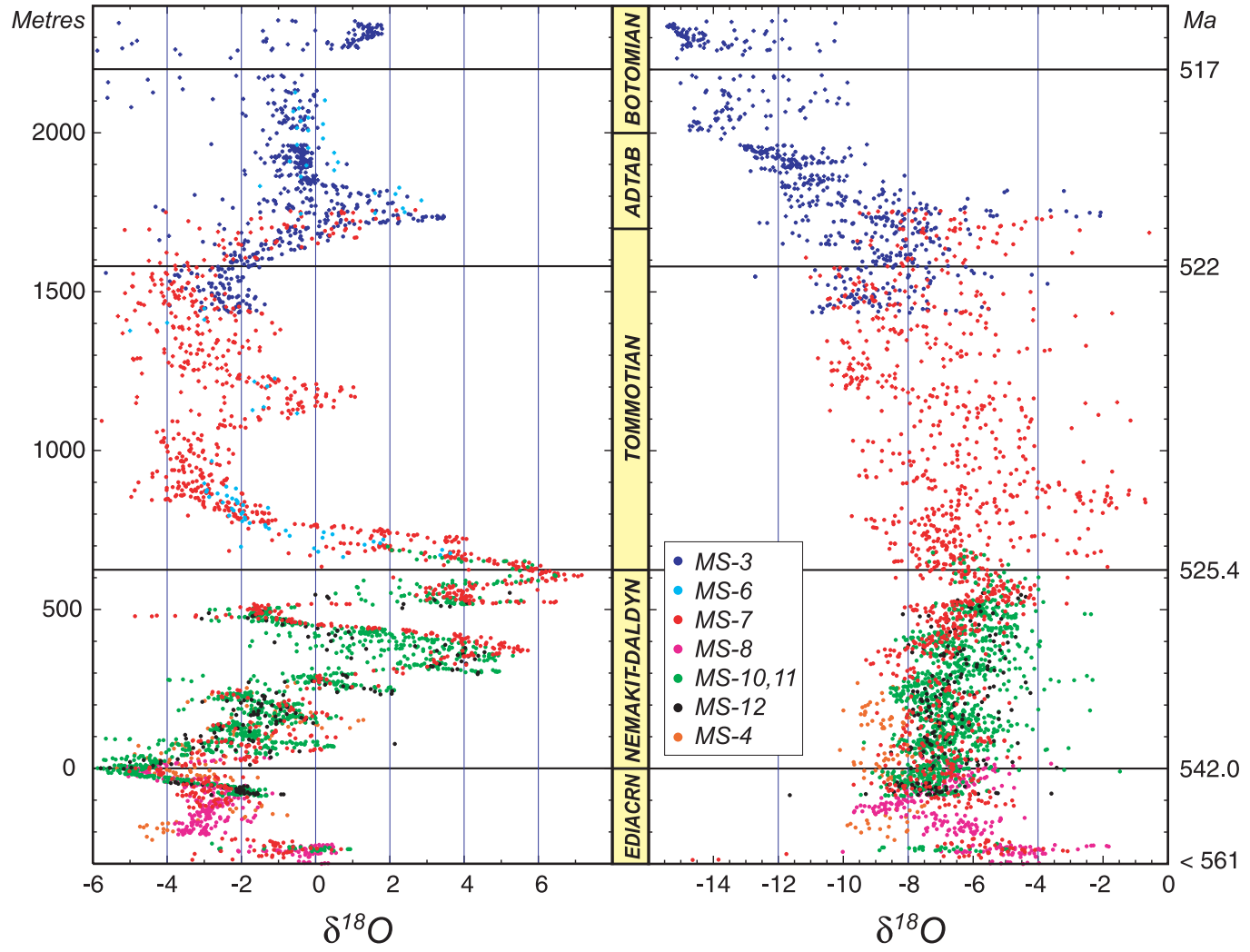

dates have been considered the best estimate of the age of a discordant population. In this case, uncertainties in the decay constants could be ignored if the dates are not compared with other chronometers. However, as it now appears that discordance related to radiation damage and Pb loss can be eliminated through the chemical abrasion technique (Mattinson 2003), we suggest that the concordia age (Ludwig 1998) may be the best estimate of the crystallization age of the zircons in our volcanic samples, and by inference, the depositional age.

U–Pb age errors are reported as follows: $\pm X/Y/Z$, where X is the internal error in absence of all systematic errors, Y includes the tracer calibration error (using 2σ standard deviation of the Pb/U in the tracer = 0.05 %), and Z includes the tracer calibration and decay constant errors of (Jaffey et al. 1971) (external errors). For $^{207}Pb/^{206}Pb$ dates, tracer errors are negligible and Y is not reported (so it reads $\pm X/Z$). The MSWD (mean square of the weighted deviates (York 1966, York 1967)) of the concordia age (Ludwig 1998) and weighted mean dates is calculated prior to the addition of systematic errors. Concordia diagrams are shown in Fig. 7 and data are presented in Table 1.

U–Pb results

Minount rhyodacite

The Minount rhyodacite (M1149) is the second youngest lava flow associated with a volcanic center to the northwest of Timjich in the uppermost Ouarzazate Group. The felsic lavas sit with angular discordance immediately below the Tabia Member at MS-10 (Fig. 3). Four of five chemically abraded grains form a statistically significant cluster (MSWD of equivalence = 0.5) that is concordant within the uncertainties of the U decay constants (Fig. 7*a*). The weighted mean $^{207}Pb/^{206}Pb$ date is 563.84 ± 0.66/4.61 Ma (MSWD = 1.0), the weighted mean $^{207}Pb/^{235}U$ date is 563.02 ± 0.23/0.51/1.27 Ma (MSWD = 0.3), the weighted mean $^{206}Pb/^{238}U$ date is 562.81±0.15/0.43/

Table 1. U-Pb isotopic data.

		Concentrations					Isotopic ratios									Dates (Ma)						
Sample[a]	Weight (μg)[b]	U (ppm)[c]	Pb (ppm)[c]	$\frac{Pb^*}{Pb_c}$[d]	Pb_c (pg)[e]	$\frac{Th}{U}$[f]	$\frac{^{206}Pb}{^{204}Pb}$[g]	$\frac{^{208}Pb}{^{206}Pb}$[f]	$\frac{^{206}Pb}{^{238}U}$[h]	%err.[i]	$\frac{^{207}Pb}{^{235}U}$[h]	%err.[i]	$\frac{^{207}Pb}{^{206}Pb}$[h]	%err.[i]	corr. coef.	$\frac{^{206}Pb}{^{238}U}$[j]	$\pm$[k]	$\frac{^{207}Pb}{^{235}U}$[j]	$\pm$[k]	$\frac{^{207}Pb}{^{206}Pb}$[j]	$\pm$[k]	%dis.[l]
M1149																						
Z5*	n.a.	n.a.	n.a.	269.0	0.45	0.29	17176	0.091	0.091138	0.05	0.740298	0.07	0.05891	0.05	0.701	562.26	0.29	562.58	0.41	563.86	1.14	0.28
Z6*	n.a.	n.a.	n.a.	91.2	1.11	0.22	5945	0.070	0.091220	0.06	0.741062	0.10	0.05892	0.08	0.613	562.75	0.32	563.02	0.56	564.13	1.71	0.25
Z7*	n.a.	n.a.	n.a.	135.5	0.25	0.26	8739	0.081	0.091232	0.06	0.740924	0.09	0.05890	0.06	0.702	562.82	0.33	562.94	0.49	563.47	1.34	0.12
Z8*	n.a.	n.a.	n.a.	734.9	0.25	0.19	48269	0.058	0.091232	0.05	0.741295	0.07	0.05893	0.05	0.667	562.82	0.27	563.16	0.41	564.55	1.19	0.31
Z9*	n.a.	n.a.	n.a.	241.8	0.45	0.22	15730	0.070	0.091235	0.05	0.740869	0.08	0.05890	0.06	0.648	562.84	0.28	562.91	0.43	563.19	1.28	0.06
M223																						
Z1	9.2	407.2	34.2	133.1	2.36	0.29	8512	0.091	0.084885	0.05	0.67812	0.08	0.05794	0.06	0.682	525.218	±0.27	525.63534	±0.40	527.47	±1.22	0.43
Z2	7.4	460.7	39.0	437.3	0.66	0.33	27652	0.103	0.084877	0.06	0.67820	0.08	0.05795	0.05	0.800	525.170	±0.32	525.68312	±0.40	527.90	±1.00	0.52
Z3	4.3	313.0	26.5	95.8	1.19	0.32	6082	0.101	0.084864	0.08	0.67768	0.11	0.05792	0.07	0.718	525.091	±0.40	525.36892	±0.56	526.54	±1.62	0.28
Z7	3.8	200.3	16.9	54.7	1.17	0.32	3488	0.099	0.084914	0.08	0.67814	0.11	0.05792	0.08	0.723	525.389	±0.41	525.64855	±0.58	526.79	±1.66	0.27
Z8	1.8	302.1	25.3	70.8	0.64	0.29	4535	0.091	0.084869	0.09	0.67801	0.15	0.05794	0.12	0.612	525.118	±0.47	525.56920	±0.80	527.55	±2.63	0.46
Z9*	n.a.	n.a.	n.a.	96.6	0.41	0.33	6107	0.105	0.084889	0.06	0.67803	0.10	0.05793	0.08	0.568	525.239	±0.29	525.58382	±0.52	527.05	±1.79	0.34
Z10*	n.a.	n.a.	n.a.	111.4	0.42	0.34	7032	0.107	0.084890	0.06	0.67799	0.12	0.05792	0.11	0.507	525.245	±0.31	525.55716	±0.66	526.88	±2.36	0.31
Z11*	n.a.	n.a.	n.a.	84.6	0.62	0.32	5381	0.100	0.084914	0.07	0.67814	0.11	0.05792	0.08	0.691	525.390	±0.38	525.65189	±0.56	526.79	±1.68	0.27

[a]Z1, Z2, etc. are labels for fractions composed of single zircon grains. *denotes grains that were subjected to the chemical abrasion technique (all others underwent mechanical abrasion).

[b]Sample weights, are estimated to within 40% using measured grain dimensions and density. Weights could not be visually estimated for grains subjected to the chemical abrasion technique.

[c]Concentrations cannot be estimated for grains that were subjected to the chemical abrasion technique.

[d]Ratio of radiogenic Pb to common Pb.

[e]Total weight of common Pb.

[f]Model Th/U ratio calculated from radiogenic $^{208}Pb/^{206}Pb$ ratio and $^{207}Pb/^{206}Pb$ age.

[g]Measured ratio corrected for spike and fractionation only. Mass fractionation corrections were based on analysis of NBS-981 and NBS-983. Correction of $\frac{0.25\%}{\text{amu}} \pm \frac{0.04\%}{\text{amu}}$ (atomic mass unit) was applied to single-collector Daly analyses performed on the Sector-54 mass spectrometer.

[h]Corrected for fractionation, spike, blank, and initial common Pb. All common Pb was assumed to be procedural blank. U blank was <0.1 pg. Measured laboratory blank composition: $^{206}Pb/^{204}Pb = 18.271 \pm 0.05$, $^{207}Pb/^{204}Pb = 15.587 \pm 0.05$, $^{208}Pb/^{204}Pb = 38.119 \pm 0.05$ (2σ).

[i]Errors are 2σ, propagated using the algorithms of Ludwig (1980).

[j]Age calculations are based on the decay constants of (Jaffey et al. 1971).

[k]Errors (%err.) are 2σ.

[l]% discordance (%dis.) $= 100 - \left(100 \times \frac{\left(^{206}Pb/^{238}U\right)\text{date}}{\left(^{207}Pb/^{206}Pb\right)\text{date}}\right)$

Fig. 6. $\delta^{13}C$ record from MS-7 plotted against detailed physical stratigraphy (see Fig. 1 for key to lithofacies and measured section location). The 4‰ spike-like drop at 480 m is superimposed on an 8‰ negative $\delta^{13}C$ excursion that likely lasted 1–2 million years.

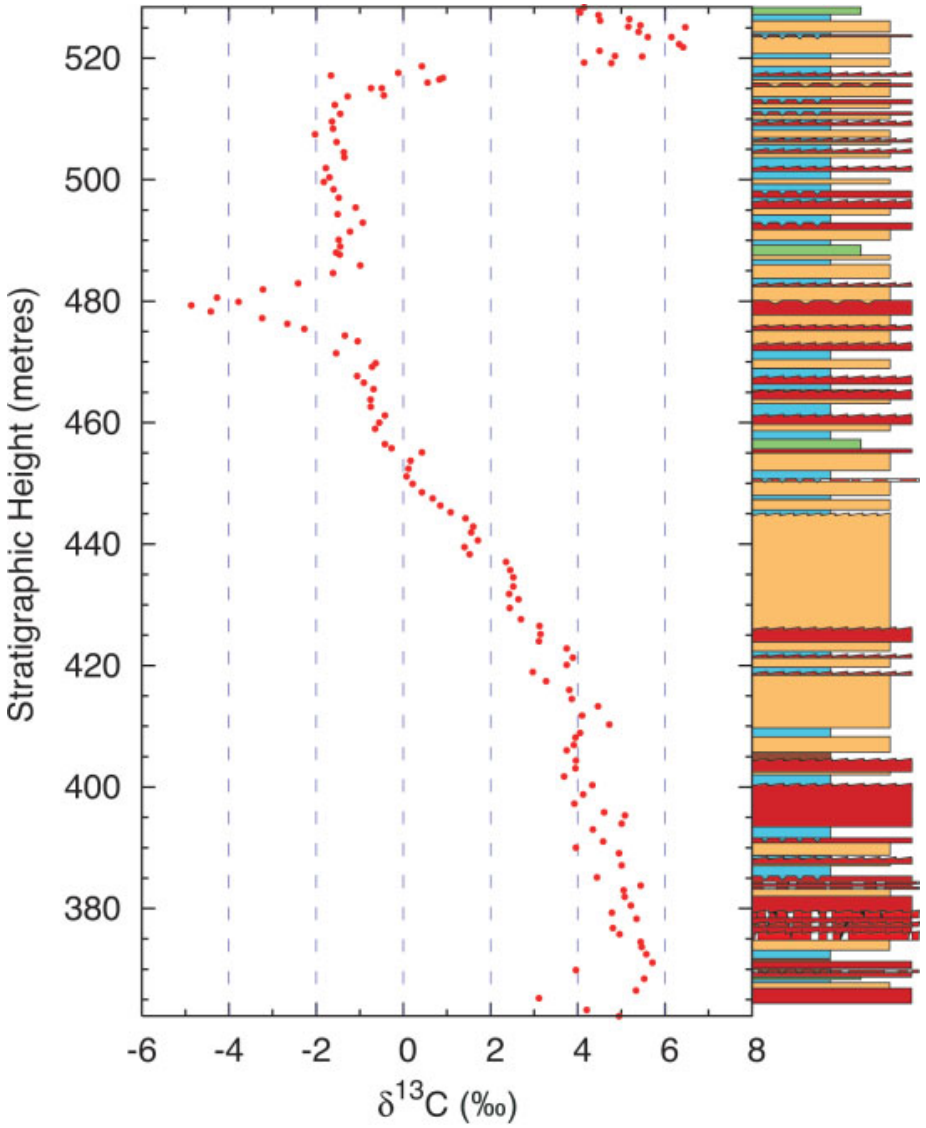

1.03 Ma (MSWD = 0.1), and the concordia age is 562.89 ± 0.49 Ma (MSWD of concordance = 0.2) (Table 1). We interpret the concordia age as the best estimate of the age of the felsic lava flow.

Upper Adoudou Formation ash

The upper Adoudou Formation ash (M223) is 60 cm thick, located at a stratigraphic height of 625 m in MS-7, and is one of at least 20 different ashes that bury stromatolitic bioherms within a 250 m interval of upper Adoudou Formation carbonates. The ashes are 1–60 cm thick, greenish, and speckled with euhedral feldspar phenocrysts. Zircons from M223 are large (150–400 μm long) and doubly terminated. Five air-abraded zircon grains and three chemical-abraded grains form a statistically significant cluster (MSWD of equivalence = 0.4) that is concordant within the uncertainties of the U decay constants (Fig. 7*b*). The weighted mean $^{207}Pb/^{206}Pb$ date is 527.28 ± 0.53/4.57 Ma (MSWD = 0.5), the weighted mean $^{207}Pb/^{235}U$ date is 525.60 ± 0.18/0.44/1.16 Ma (MSWD = 0.1), the weighted mean $^{206}Pb/^{238}U$ date is 525.23±0.12/0.38/0.94 Ma (MSWD = 0.3), and the concordia age is 525.38 ± 0.46 Ma (MSWD of concordance = 0.7) (Table 1). We interpret the concordia age as the best estimate of the age of the upper Adoudou ash. It is noteworthy that the strongly abraded grains and the chemically treated grains yield identical results.

Discussion

Age model

The lack of *Treptichnus* and other diagnostic earliest Cambrian trace fossils in the Adoudou Formation (likely due to the dearth of suitable marine siliciclastic facies) prevents an exact correlation with the stratotype section in Newfoundland, where the Precambrian–Cambrian boundary is defined. However, the $\delta^{13}C$ excursion to –6‰ coincident with the first appearance of

Fig. 7. U–Pb concordia diagrams for (A) the upper Ouarzazate Group Minount Rhyodacite (M1149) and (B) the upper Adoudou Formation ash bed (M223). Light gray band is the concordia curve error envelope using U decay constants and 95% confidence intervals from (Jaffey et al. 1971). Dark grey analysis in diagram for M1149 is not used in the concordia age. Plotted with ISOPLOT (Ludwig 1991). Error ellipses are plotted at 2σ with internal errors only.

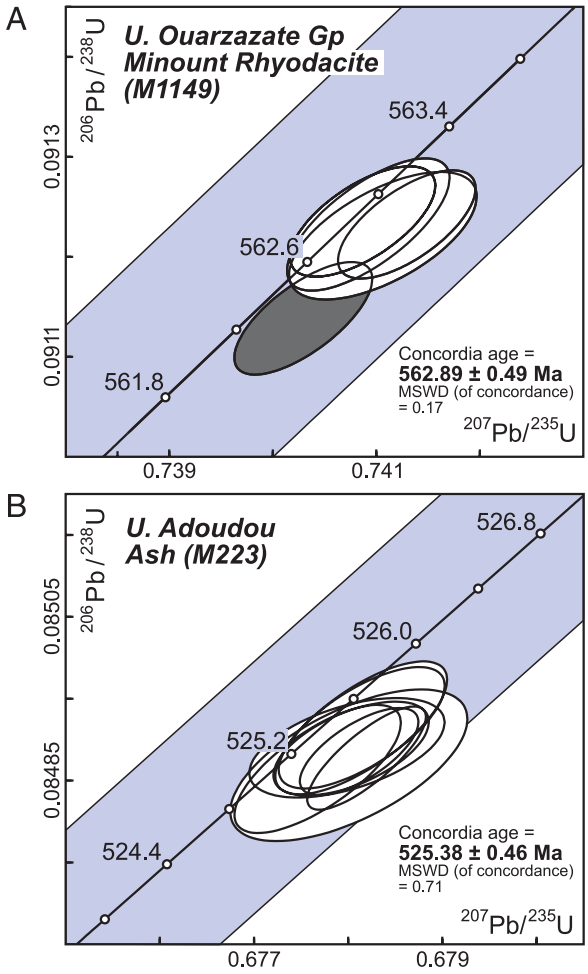

Treptichnus in Siberia and Death Valley, has come to be considered a reliable indicator of the Ediacaran–Cambrian boundary worldwide (Amthor et al. 2003, Grotzinger et al. 1995, Knoll and Carroll 1999, Kimura and Watanabe 2001) and is dated precisely at 542.0 ± 0.6 Ma (Amthor et al. 2003). Detailed comparison of a paleontoligcally calibrated composite Siberian chemostratigraphy with the Moroccan δ^{13}C record (Fig. 8) suggests that the –6‰ nadir at the base of the Tifnout Member (0 m, Fig. 5) is the Ediacaran–Cambrian boundary, and that the +7‰ high in the upper Tifnout Member (600 m, Fig. 5 and I' of (Knoll et al. 1995*b*, Kaufman et al. 1996)) corresponds to the Nemakit-Daldyn–Tommotian boundary. Our ~525.5 Ma age for the Nd–Tm boundary is consistent with previous interpretations of a pre-Tommotian ash from New Brunswick, Canada dated at 530.7 ± 0.9 Ma (Isachsen et al. 1994) and a clast from a conglomerate below the lower Tommotian in Siberia dated at 534.6 ± 0.5 Ma, (Bowring et al. 1993) (Fig. 8).

In Fig. 8, we assume constant sediment accumulation rates between the 542 Ma –6‰ nadir and 525.4, 522, and 517 Ma U–Pb zircon tie points. Admittedly, this age model is oversimplified and likely incorrect in detail. However, after applying similarly conservative linear stretches of individual Siberian sections below and above the sub-Tommotian unconformity, we find that the Siberian and Moroccan records may be correlated even down to the level of individual δ^{13}C oscillations.

δ^{13}C variability

One of the most striking features in the carbon isotope record from the Anti-Atlas is the coherent, cyclic variation of δ^{13}C over various amplitudes and model time scales.

T≤10^5 years

At periods ≤10^5 years, 1‰–3‰ variability is common in the record. Although this variability resembles scatter in summary diagrams like Fig. 8, structured cycles are common where sampling resolution is high enough (Fig. 6). Similar δ^{13}C cycles of 1‰–2‰ amplitude occurred in response to glacial–interglacial fluctuations in productivity (Broecker and Peng 1982) and pCO_2 (Spero et al. 1997) during the Pleistocene. However, ice-age variability is not expected during the Early Cambrian because no glacial deposits have been recorded from any continents of that age (Hambrey and Harland 1981). Furthermore, the ~5% weaker sun at ~530 Ma (e.g., Bahcall et al. 2001) and associated higher pCO_2 during the Cambrian would have created a larger marine reservoir of dissolved inorganic carbon (DIC), both dampening and delaying the response of δ^{13}C to changes in productivity and pCO_2 (Bartley and Kah 2004) and making it even more difficult to explain this variability. Nevertheless, even with a larger DIC pool and the absence of some of the climatic amplifiers associated with the growth and decay of ice, wet–dry and (or) warm–cool cycles could have caused short-term variability in nutrient delivery, primary productivity, and δ^{13}C.

An apparently isolated, or at least amplified δ^{13}C negative spike at ca. 529 Ma (Fig. 8; or 480 m, Fig. 6) is reminiscent of the Paleocene–Eocene thermal maximum (PETM). The PETM δ^{13}C excursion has been modeled as an abrupt release of 1100–2100 Gt of continental slope methane hydrates ($\delta^{13}C_{methane} \approx$ –60‰) to the water column (e.g., Dickens et al. 1995). However, recent work has suggested that the volume of methane necessary to explain the PETM δ^{13}C data (*a*) may not have been available during the late Paleocene (Buffett and Archer(2004), and (*b*) may not have been sufficient to cause the prolonged (~50–200 ka) global warming and deep ocean acidification observed at the PETM (Zachos et al. 2003, Zachos et al. 2004). Higgins and Schrag[3] suggest that a rapid release of 5000 Gt of organic carbon ($\delta^{13}C_{org} \approx -25$‰) from a suddenly isolated and desiccated epicontinental seaway could better explain observations at the PETM. Whether the source is methane or organic carbon, marine or terrestrial, the dynamic release of large volumes of isotopically depleted carbon seems to be required to explain PETM-like δ^{13}C excursions.

[3]Higgins, J.A. and Schrag, D.P. Causes and Consequences of the Paleocene–Eocene Thermal Maximum. Earth and Planetary Science Letters. In review.

T*≥*10*^{6} *years

On >100 ka time scales, negative shifts of even a few per mil are difficult to explain with the methane or organic carbon release scenarios because finite reservoirs are quickly depleted. For intervals significantly greater than the relaxation time of the ocean–atmosphere carbon cycle (presently ~10^5 years (Des Marais 1997, Holser et al. 1988)), a carbon-isotopic mass balance for the bulk Earth can be written

$$[1] \qquad \delta^{13}C_v = \left(1 - f_{org}\right)\delta^{13}C_c + \left(f_{org}\right)\left(\delta^{13}C_c - \varepsilon\right)$$

where $\delta^{13}C_v$ is the isotopic composition of the mantle, $\delta^{13}C_c$ is the isotopic composition of the inorganic carbon pool in the ocean derived from silicate weathering, ε is the fractionation between DIC and dissolved organic carbon (DOC) (mostly due to the kinetic isotope effect associated with the uptake of carbon by photoautotrophs), and $f_{org} = \frac{C_{org}}{C_{total}}$ is the fraction of carbon buried that is organic (Kump 1991, Hayes et al. 2001). Changes in f_{org} will cause shifts in $\delta^{13}C$ by relying on changes in the fluxes, rather than changes in finite reservoirs. Some authors have suggested that methane hydrates also may play a role in such long-term $\delta^{13}C$ variability (Dickens 2003). However, the production of methane hydrate from organic carbon in sediments always will be small relative to the organic matter burial needed to sustain such methanogenesis, so the isotopic budget on long times scales will be dominated by organic matter burial.

Over the ≥200 000 years time scale required to achieve carbon-isotopic steady state, phosphate (PO_4^{3-}) is likely to be the limiting nutrient for primary productivity (Broecker and Peng 1982, Smith 1984, Lenton and Watson (2000, Tyrrell 1999, Schrag et al. 2002). It follows that the burial of organic carbon is controlled by the riverine flux of PO_4^{3-} to the ocean and the carbon to phosphorous (C:P) ratio of organic carbon that is buried (Kump 1988, Schrag et al. 2002). As pointed out by (Schrag et al. 2002) and (Junge et al. 1975), an increase in silicate weathering would lead to an increase in the flux of both riverine PO_4^{3-} and alkalinity to the oceans, enhancing the burial of organic and carbonate carbon in approximately equal proportions and keeping f_{org} the same. This argument suggests that positive $\delta^{13}C$ swings in the Early Cambrian ocean must have been driven by increasing the C:P ratio in buried organic matter. Barring large fluctuations in the Redfield ratio (C:P in marine organic matter today is 106:1) of primary organic matter, the C:P ratio of buried C_{org} depends sensitively on the state of oxygenation at the burial site, with local anoxia favoring remobilization of PO_4^{3-} and efficient burial of low C:P organic carbon (Ingall and VanCappellen 1990, Ingall et al. 1993, VanCappellen and Ingall 1996, Ingall and Jahnke 1997). In order to change f_{org}, coupled sites of rapid organic carbon burial and local anoxia are needed to lower C:P substantially in globally averaged sedimentary organic carbon.

Today, ~70% of the total organic carbon removed from the global ocean–atmosphere–terrestrial biosphere system is buried in the sediments of large tropical river deltas, such as the Amazon and those in southeast Asia (Hedges and Keil 1995, Berner 1982). Although some of the organic carbon that is buried was derived as particulate terrestrial organic matter carried as suspended load to the ocean, much of the organic carbon that is buried is marine in origin (Aller et al. 1996). Tropical river systems drain catchments undergoing rapid silicate weathering due to the positive temperature and moisture dependence of chemical weathering rates (Berner et al. 1983). These rivers deliver abundant nutrients to the ocean assuring high productivity. The same rivers also provide huge volumes of physically weathered sediment, some of which adsorbs to particulate organic matter in the water column (Keil et al. 1994, Mayer 1999) and buries it before it can be oxidized. Even in the absence of a substantial terrestrial biosphere during the Early Cambrian, tropical river deltas would still have been a dominant site for organic carbon burial.

Consider a tropical river delta emptying into a restricted, Tethys-like basin. When the bottom water is anoxic, C:P in buried sediments will be very high, PO_4^{3-} will be recycled into the water column allowing primary productivity to increase until some other nutrient, such as iron or nitrate becomes limiting, and atmospheric pO_2 will rise as photosynthesis continues without fully balanced reoxidation of organic carbon. Eventually, atmospheric oxygen rises to levels sufficient to ventilate bottom waters, increase C:P in buried sediments, and reinstate PO_4^{3-} as the limiting nutrient (VanCappellen and Ingall 1996). During high C:P times, $\delta^{13}C$ is high and phophorites are deposited around the world. During low C:P intervals, $\delta^{13}C$ is low and PO_4^{3-} is scarce. C:P switching appears to have controlled f_{org} on different time scales, cycling with a period of 1–1.5 million years at 543–535 Ma and 525–520 Ma, but dominated by larger amplitude fluctuations with a period of 4–7 million years at 535–526 Ma (Fig. 8). In addition to the pO_2 negative feedback, f_{org} may be modulated by a variety of processes, such as climate, biological activity, and the quantity and type of clay entering the basin (Kennedy et al. 2002), perhaps explaining the presence of multiple characteristic time scales in the $\delta^{13}C$ record.

Although C:P switching could be a plausible mechanism for changing $\delta^{13}C$ on million year time scales, large swings in f_{org} may be linked to changes in F_{org} (the burial rate of organic carbon), which is in turn coupled to atmospheric pCO_2 and climate. During the End-Ordovician and Silurian, a series of positive $\delta^{13}C$ excursions (e.g., Saltzman and Young 2005, Cramer and Saltzman 2005, Saltzman 2002, Saltzman 2001, Marshall et al. 1997, Long 1993) superficially resemble the Early Cambrian $\delta^{13}C$ excursions from Morocco. Saltzman et al. (2005) proposed that these Ordovician–Silurian positive $\delta^{13}C$ excursions are coincident with warm intervals and are sandwiched between ice age periods with $\delta^{13}C \approx 0$. If the association between $\delta^{13}C$ and cool–warm intervals is correct, positive $\delta^{13}C$ shifts may be accompanied by increasing F_{org}, decreasing pCO_2, and increasing pO_2 until the climate cools sufficiently for glaciers to advance. Saltzman et al. (2005) suggest that cooling could cause an invigoration of the thermohaline circulation and the ventilation of bottom waters, decreasing C:P in sediments and driving F_{org}, f_{org} and $\delta^{13}C$ down, as part of a negative feedback between pCO_2 and the C:P switch. Kump et al. (1999) suggest an alternative scenario for the End-Ordovician glaciation, where the positive $\delta^{13}C$ excursion is caused by increased weathering of shelf-carbonate rocks during syn-glacial sea-level lowstand (increased weathering of shelf carbonates could also occur in response to tectonic uplift of carbonate platforms). Furthermore, Kump (1993) found that large positive shifts in $\delta^{13}C$ are most likely to occur when total carbon throughput and F_{org} are low, but f_{org} is high. Under these conditions, Kump (1993) showed

Fig. 8. Carbon isotopes plotted against age. The age model for the Moroccan data (black circles) assumes constant sediment accumulation rates between U–Pb zircon tie points (squares: red = Morocco, orange = Avalon, blue = Siberia, green = Oman, and brown = Namibia). Each group of colored circles represents $\delta^{13}C$ data from a different stratigraphic section on the Siberian craton (yellow: Khorbusuonka river section, Olenek Uplift (Knoll et al. 1995*a*); purple: Sukhaya Tunguska river section, Turukhansk Uplift (Bartley et al. 1998); green: Kotuikan river section, Anabar Uplift (Knoll et al. 1995*b*, Kaufman et al. 1996); dark blue: Dvortsy, Aldan river, Aldan Shield (Magaritz et al. 1991); orange: Bol'shaya-Kuonamka section, Anabar Uplift (Kouchinsky et al. 2001); light blue: Isit section, Lena river, Aldan Shield (Magaritz et al. 1991); and light pink: Zhurinsky Mys, Lena river, Aldan Shield (Kirschvink et al. 1991)). Sediment accumulation rates through each data set were chosen to improve the fit between stratigraphic sections. Horizontal gaps within individual data sets represent intervals of depositional hiatus or siliciclastic sedimentation (note, for example, that the $\delta^{13}C$ peak in Bol'shaya-Kuonamka at 519 Ma is a siliciclastic interval in Morocco). In the plot of biodiversity of small shelly fossils, the thin black line reflects the number of genera present in non-phosphatizing preservation modes, compared with the much thicker dark grey area that represents the total number of genera preserved (Porter 2004).

that changes in pCO_2 during positive shifts in $\delta^{13}C$ may be small, and pCO_2 might not act as a strong negative feedback on C:P switching. When searching for models to explain the Moroccan $\delta^{13}C$ data, it is important to remember that, in the Early Cambrian, there is no evidence for glaciation, so F_{org} must have been constrained to vary within certain limits that never led to pCO_2 decreases sufficient to plunge the Earth into an ice age.

Another puzzling aspect of the 10^6 year variability in $\delta^{13}C$ is that the isotope shifts are often extremely rapid, sometimes appearing to take place in just a few hundred thousand years. The most conspicuous example is the 6‰ rise at ~529 Ma that spans just 20 m of stratigraphy in three different sections (MS-7,MS-11, and MS-12) and is not associated with any evidence for significant erosion or depositional hiatus. Rothman et al. (2003) suggested that large fluctuations in $\delta^{13}C$ observed in the Neoproterozoic could be attributed to non-steady-state (dynamic) interactions between the marine DIC pool and an unusually large, deep ocean DOC reservoir that was mixed periodically with the surface ocean (e.g., Grotzinger and Knoll 1995). This mechanism is analogous to the non-steady state methane or C_{org} release scenarios discussed above for $<10^5$ year time scales, but potentially could explain large and repeated negative excursions in $\delta^{13}C$ because of the huge size of the proposed DOC pool. However, it is more difficult to explain rapid positive $\delta^{13}C$ excursions because there are no large reservoirs with very high $\delta^{13}C$ that can be released and allowed to equilibrate with the water column. Dynamic positive excursions possibly could be achieved if primary productivity were allowed to greatly exceed respiration, if ε itself were allowed to fluctuate under the influence of different biological pathways, or if short pulses of carbonate weathering were allowed to modify the isotopic composition of the ocean. Another complication is that, given the existing global database of coupled $\delta^{13}C_{carbonate}$ and $\delta^{13}C_{organic}$ measurements, Rothman et al. (2003) has suggested that the very large Neoproterozoic DOC pool was destroyed by ~542 Ma, rendering the Early Cambrian world less susceptible to dynamic DOC–DIC interactions.

$\delta^{13}C$ and biodiversity

The only other time in Earth history that is characterized by million year $\delta^{13}C$ variability of such large amplitude is the Early Triassic (Payne et al. 2004). In the ca. 4.4 million year period immediately following the most severe extinction in the Phanerozoic, four $\delta^{13}C$ cycles of 4‰–10‰ amplitude coincide with an extreme reduction in the size of carbonate secreting metazoa (Payne et al. 2004). The return to flatline $\delta^{13}C$ corresponds neatly to the first appearance of large calcified gastropods. What is the link, if any, between the abundance of skeletal organisms and the stability of the global carbon cycle? The Ediacaran–Cambrian extinction also involves the last appearance of a group of weakly calcifying metazoa (Amthor et al. 2003), which, although low in diversity, are locally abundant and may or may not have been important to the global carbon cycle. Furthermore, although the Nemakit-Daldyn, Tommotian, and Adtabanian all witness increases in the size and diversity of carbonate secreting organisms (Fig. 8), it may not have been until the end of the Early Ordovician that metazoa began to account for a large fraction of the ocean's carbonate burial.

Damping of the $\delta^{13}C$ oscillations in the Early Cambrian (see also, Brasier and Sukhov 1998, Brasier et al. 1994) also coincides with the first appearance of abundant deep burrowing and well-developed ichnofacies (Bottjer et al. 2000, Orr et al. 2003, Droser et al. 1999, Droser et al. 2002). However, C:P switching requires anoxic bottom waters, not just anoxic sediments, so the link between bioturbators in oxic–suboxic environments and their effect on redox conditions in the water column and C:P switching is not straight forward. Furthermore, an explanation for the apparent lack of 1 million year cyclic $\delta^{13}C$ oscillations in the Precambrian must be sought. Could the existence of a much larger DIC pool in the past (when elevated atmospheric pCO_2 was required to combat the faint young sun) have increased the residence time of carbon in the ocean sufficiently to dampen the $\delta^{13}C$ response to C:P switching on the 1 million year time scale? Would reduced Precambrian atmospheric pO_2 have increased the characteristic time scales for C:P switching or even made C:P switching impossible? Much longer period shifts (10–100 million years) in $\delta^{13}C$ during the late Proterozoic also are thought to be related to nutrient cycling, but are probably modulated by changes in paleogeography (Maloof 2004, Schrag et al. 2002).

Perhaps one of the more fundamental characteristics of era-ending mass extinctions (Ediacaran–Cambrian, Permian–Triassic, and Cretaceous–Tertiary) is that the biotic crises represent full ecological resets and permanent reductions in the proportion of metazoan that are incapable of buffering their own internal fluids against environmental change (Bambach et al. 2002). What specific role do physically unbuffered taxa play in the global carbon cycle, and is their stepwise decrease in relative abundance through the Phanerozoic linked to the reduction in magnitude and length of associated $\delta^{13}C$ disturbances? Does the ecological freedom transiently present in the

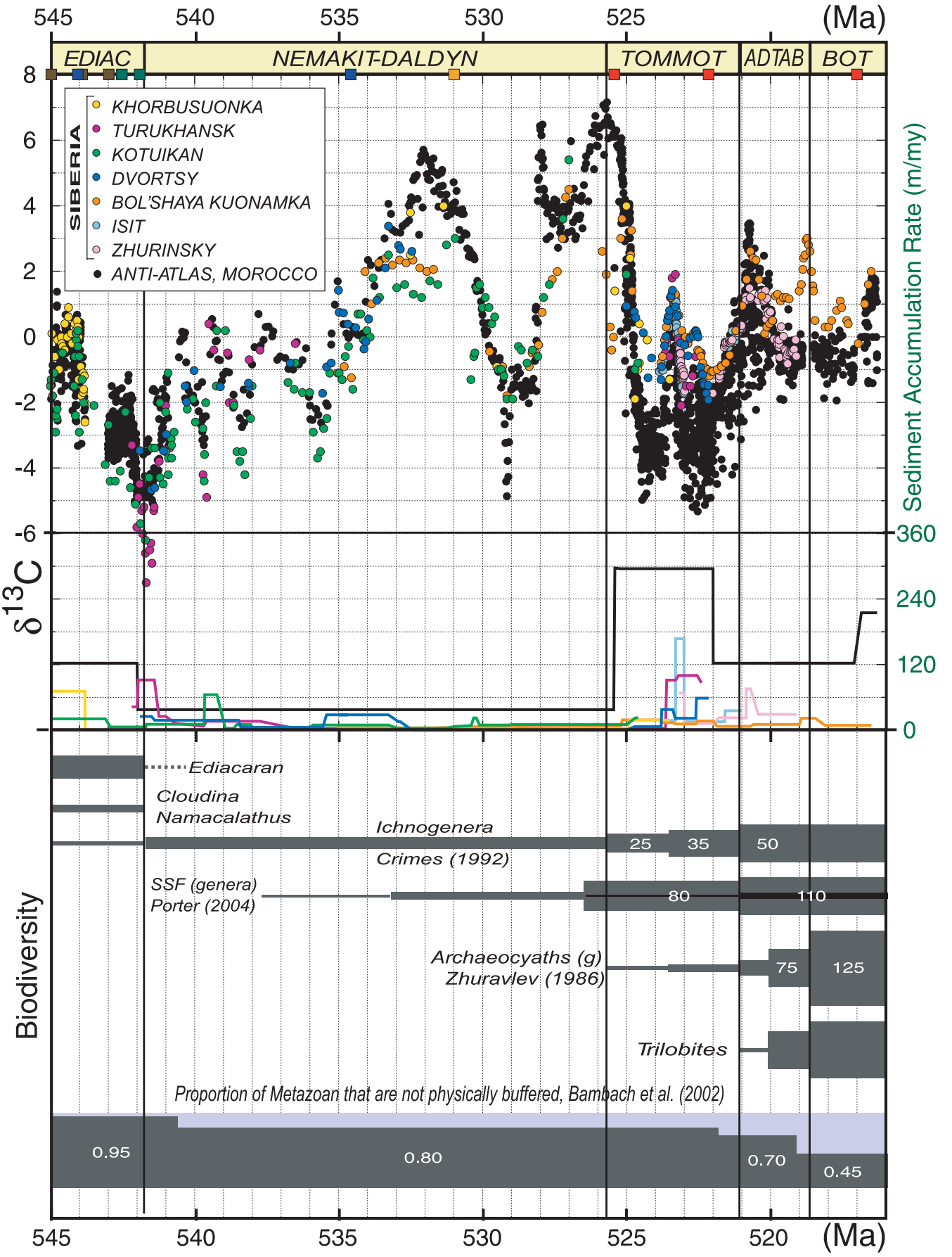

aftermath of mass extinctions exert any control on the volatility of the carbon cycle? $\delta^{13}C$ excursions during intervals of low biotic diversity commonly are thought to reflect environmental perturbations that inhibited biotic recovery. However, the similarity between Early Cambrian and Early Triassic $\delta^{13}C$ records suggests that perhaps biology plays a more direct roll in controlling the carbon cycle. Calibrating fossiliferous Early Cambrian records with the Moroccan $\delta^{13}C$ curve could help determine the importance of ecological controls on fractional organic carbon burial and the redox state of the ocean.

Conclusions

In this contribution, a new tectonostratigraphic and isotopic record of the evolution of the Ediacaran – Early Cambrian Anti-Atlas margin was presented. A detailed $\delta^{13}C$ curve from fifteen measured stratigraphic sections was placed in a temporal framework by using high-precision U–Pb zircon geochronology of ash beds in the same sections. By sampling carbonate sediments at very high resolution (0.2–1.5 m intervals), coherent $\delta^{13}C$ variability with characteristic time scales $<10^5$ years was observed. Variations in the $\delta^{13}C$ of carbonate were shown to occur on a wide range of time scales, suggesting that different mechanisms are involved, including, but not restricted to, non-steady state processes, such as methane hydrate and organic carbon release on short ($<$100 000 year) time scales and steady state changes in nutrient recycling and organic carbon burial on longer ($\geq$1 000 000 year) time scales. Through a correlation with more fossiliferous, albeit condensed, sections in Siberia, the pattern of cyclic $\delta^{13}C$ variation was discussed in the context of the reappearance and diversification of carbonate secreting metazoa during the Early Cambrian. It is encouraging for studies of climate variability and metazoan evolution that, with high resolution sample collection strategies, coherent, very short-lived $\delta^{13}C$ events are recoverable in detail from Cambrian sediments.

Acknowledgments

Field and stable isotope work was supported by National Science Foundation (NSF) Geology & Paleontology Program grant EAR-0417422 and Earth System History Program (ESHP) grant EAR-9905495 to P.F. Hoffman, the NASA Astrobiology Institute, the Canadian Institute for Advanced Research (Earth System Evolution Project), and NSF grant EAR-9725577 to J.L. Kirschvink. Geochronology was supported by ESHP grant EAR-9905478 to S.A. Bowring and the NASA Astrobiology Institute. The manuscript benefited from useful discussions with David Barbeau, Michael Bender, David Evans, Charles Ferguson, David Fike, Woody Fisher, Pieter Gresse, John Grotzinger, Galen Halverson, Paul Hoffman, Matt Hurtgen, Hiroto Kimura, Joe Kirschvink, Andy Knoll, Ed Landing, Jonathon Payne, Susannah Porter, Tim Raub, Daniel Rothman, Matthew Saltzman, and Danny Sigman. Thoughtful reviews were provided by Lee Kump and Martin Brasier. Pascale Poussart assisted with Fig. 1. Mohamed Mazouad, Miloud Aarar, Rashid Adil, Jay Ewing, Ryan Ewing, and Matt Kuharic provided assistance in the field. Mohammed Laami, Allel Masbahi, Driss Najid and family, Mohammed Saghi, and many others at l'Institute Scientifique, along with Mohammed Boutakiout at l'Université Mohammed V, provided political and logistical support in Rabat. Pascale Poussart, Patrice Lannez, and Anne Bozion assisted with logistics in France. Heather Borkowski, Lauren Chetel, Chris Deely, Jay Ewing, Anna Graefe, Guy Hoffman, Karla Knudsen, and Devin McPhillips helped with sample preparation, while Ethan Goddard and Greg Eischeid supervised isotope laboratory work at Harvard University. Jahan Ramezani and Mark Martin of the Radiogenic Isotope Lab at MIT did some of the initial work on the ashes from Morocco. Louise Ragno helped find obscure references in international libraries. John Kovacs supplied photographic equipment and advice. Paul Hoffman provided inspiration.

References

Aït Malek, H., Gasquet, D., Bertrand, J.-M., and Leterrier, J. 1998. Géochronologie U–Pb sur zircon de granitoïdes éburnéens et panafricains dans les boutonnières protérozoïques d'Igherm, du kerdous et du Bas Drâa (Anti-Atlas occidental, Maroc). Comptes Rendues Geoscience, **327**: 819–826.

Algouti, A., Algouti, A., Beauchamp, J., Chbani, B., and Taj-Eddine, K. 2000. Paléogéographie d'une plateforme infracambrienne en dislocation: série de base adoudounieene de la région Waoufengha-Igherm, Anti-Atlas occidental, Maroc. Comptes Rendues Geoscience, **330**: 155–160.

Algouti, A., Algouti, A., Chbani, B., and Zaim, M. 2001. Sedimentation et volcanisme synsédimentaire de la série de bas de l'adoudounian infra-cambrien à travers deux exemples de l'Anti-Atlas du Maroc. Journal of African Earth Sciences, **32**(4): 541–556.

Aller, R., Blair, N., Xia, Q., and Rude, P. 1996. Remineralization rates, recycling, and storage of carbon in Amazon shelf sediments. Continental Shelf Research, **16**: 753–786.

Amthor, J., Grotzinger, J., Schröder, S., Bowring, S., Ramezani, J., Martin, M., and Matter, A. 2003. Extinction of *Cloudina* and *Namacalathus* at the Precambrian-Cambrian boundary in Oman. Geology, **31**(5): 431–434.

Azizi Samir, M., Ferrandini, J., and Tane, J. 1990. Tectonique et volcanisme tardi-Pan Africains (580-560 Ma) dans l'Anti-Atlas Central (Maroc): interpretation géodynamique à l'échelle du NW de l'Afrique. Journal of African Earth Sciences, **10**(3): 549–563.

Bahcall, J., Pinsonneault, M., and Basu, S. 2001. Solar models: current epoch and time dependences, neutrinos, and heleoseismological properties. Astrophysical Journal, **555**: 990.

Bailey, R. 1998. Review: Stratigraphy, meta-stratigraphy and chaos. Terra Nova, **10**: 222–230.

Bambach, R., Knoll, A., and Sepkowski, J. 2002. Anatomical and ecological constraints on Phanerozoic animal diversity in the marine realm. Proceedings of the National Academy of Sciences of the United States of America, **99**: 6854–6859.

Banner, J., and Hanson, G. 1990. Calculation of simultaneous isotopic and trace element variations during water–rock interaction with applications to carbonate diagenesis. Geochimica Cosmochimicha Acta, **54**: 3123–3137.

Bartley, J., and Kah, L. 2004. Marine carbon reserovir, C_{org}–C_{carb} coupling, and the evolution of the Proterozoic carbon cycle. Geology, **32**(2): 129–132.

Bartley, J., Pope, M., Knoll, A., Semikhatov, M., and Petrov, P. 1998. A Vendian–Cambrian boundary succession from the northwestern margin of the Siberian Platform: stratigraphy, palaeontology,

chemostratigaphy and correlation. Geological Magazine, **135**(4): 473–494.

Beauchamp, W., Allmendinger, R., Barazangi, M., Demnati, A., El Alji, M., and Dahmani, M. 1999. Inversion tectonics and the evolution of the Hight Atlas Mountains, Morocco, based on a geological–geophysical transect. Tectonics, **18**(2): 163–184.

Benssaou, M., and Hamoumi, N. 1999*a*. L'Anti-Atlas occidental du Maroc: remplissage sédimentaire d'un basin de type rift intracontinental au Cambrien inférieur. Géologie Méditerranéenne, **3/4**: 259–279.

Benssaou, M., and Hamoumi, N. 1999*b*. Le Protérozoïque terminal – Cambrien inférieur de l'Anti-Atlas occidental (Maroc): évolution sédimentologique et implications géodynamiques. Africa Geoscience Review, **6**(4): 361–379.

Benssaou, M., and Hamoumi, N. 1999*c*. Paléoenvironnements et minéralisations de l'Anti-Atlas occidental marocain au Cambrien précoce. Chronique de la Recherche Minière, **536-537**: 113–119.

Benssaou, M., and Hamoumi, N. 2001. L'Anti-Atlas occidental du Maroc: étude sédimentologique et reconstructions paléogéographiques au Cambrien inférieur. Journal of African Earth Sciences, **32**(3): 351–372.

Benssaou, M., and Hamoumi, N. 2003. Le graben de l'Anti-Atlas occidental (Maroc): contrôle tectonique de la paléogéographie et des séquences au Cambrien inférieur. Comptes Rendues Geoscience, **335**: 297–305.

Benziane, F., Prost, A., and Yazidi, A. 1983. Le passage du Précambrien au cambrien précoce volcanique et sédimentaire de l'Anti-Atlas oriental; comparisons avec l'Anti-Atlas occidental. Bulletin de la Societé géologique Français, **4**: 549–556.

Berner, R. 1982. Burial of organic carbon and pyrite sulfur in the modern ocean: Its geochemical and environmental significance. American Journal of Science, **282**: 451–473.

Berner, R., Lasaga, A., and Garrels, R. 1983. The carbonate–silicate geochemical cycle and its effects on atmospheric carbon dioxide over the past 100 million years. American Journal of Science, **283**: 641–683.

Bertrand-Safarti, J. 1981. Problème de la limite Précambrien–Cambrien: la section de Tiout (Maroc); les stromatolites et leur biostratigraphie (Schmitt, 1979): critiques et observations. Newsletters on Stratigraphy, **10**: 20–26.

Boher, M., Abouchami, W., Michard, A., Albarede, F., and Arndt, N. 1992. Crustal growth in West Africa at 2.1 Ga. Journal of Geophysical Research, **97**(B1): 345–369.

Bottjer, D., Hagadorn, J., and Dornbos, S. 2000. The Cambrian substrate revolution. GSA Today, **10**(9): 1–7.

Boudda, A., Choubert, G., and Faure-Muret, A. 1979. Essai de stratigraphie de la couverture sedimentaire de l'Anti-Atlas: Adoudounien – Cambrien inférieur. Notes et Mémoires du Service Géologique du Maroc, **261**: 96.

Bouougri, E. 2003. The Moroccan Anti-Atlas: the West African craton passive margin with limited Pan-African activity. Implications for the northern limit of the craton. Precambrian Research, **120**: 179–183.

Bouougri, E., and Saquaque, A. 2000. Organisation stratigraphique et structure de la marge Anti-Atlasique du craton Ouest-Africain au sud du Siroua (Néoproterozoïque, Anti-Atlas central, Maroc). Comptes Rendues Geoscience, **330**: 753–759.

Bowring, S., Grotzinger, J., Isachsen, C., Knoll, A., Pelechaty, S., and Kolosov, P. 1993. Calibrating rates of Early Cambrian evolution. Science, **261**: 1293–1298.

Brand, U., and Veizer, J. 1981. Chemical diagenesis of a multicomponent carbonate system — 1: stable isotopes. Journal of Sedimentary Petrology, **51**: 987–997.

Brasier, M. 1995. The basal Cambrian transition and Cambrian bioevents. *In* Global Events and Event Stratigraphy in the Phanerozoic. *Edited by* O. Walliser. Springer, Berlin, Germany, pp. 113–138.

Brasier, M., and Sukhov, S. 1998. The falling amplitude of carbon isotopic oscillations through the Lower to Middle Cambrian: northern Siberia data. Canadian Journal of Earth Science, **35**: 353–373.

Brasier, M., Corfield, R., Derry, L., Rozanov, Z. Y., and Zhuravlev, A. Y. 1994. Multiple $\delta^{13}C$ excursions spanning the Cambrian explosion to the Botomian crisis in Siberia. Geology, **222**: 455–458.

Braun, J., and Beaumont, C. 1989*a*. Contrasting styles of lithospheric extension: Implications for differences between the Basin and Range province and rifted continental margins. AAPG Memoir, **46**: 53–79.

Braun, J., and Beaumont, C. 1989*b*. A physical explanation of the relation between flank uplifts and the breakup unconformity at rifted continental margins. Geology, **17**: 760–764.

Broecker, W., and Peng, T.-H. 1982. Tracers in the Sea. Eldigio Press, Lamont Doherty Geological Observatory, New York.

Buffett, B., and Archer, D. 2004. Global inventory of methane clathrate: sensitivity to changes in the deep ocean. Earth and Planetary Science Letters, **227**: 185–199.

Buggisch, W., and Flügel, E. 1988. The Precambrian-Cambrian boundary in the Anti-Atlas (Morocco). Discussion and new results. *In* The Atlas System of Morocco: Studies on its Geodynamic Evolution. *Edited by* V. Jacobshagen. Lecture Notes in Earth Sciences Vol. 15, Springer-Verlag, Berlin, Germany, pp. 81–90.

Buggisch, W., and Heinitz, W. 1984. Slumpfolds and other early deformations in the early Cambrian of the Western and Central Anti-Atlas (Morocco). Geologische Rundschau, **73**: 809–819.

Cartig, S., Burkhard, M., Ducommun, R., Helg, U., Kopp, L., and Sue, C. 2004. Fold interference patterns in the Late Palaeozoic Anti-Atlas belt of Morocco. Terra Nova, **16**(1): 27–37.

Chbani, B., Beauchamp, J., Algouti, A., and Zouhair, A. 1999. Un enregistrement sédimentaire éocambrien dans un bassin intracontinental en distension: le cycle « conglomérats de base – unité calcaire – grés Tikirt » de Bou Azzer El Graara (Anti-Atlas central, Maroc). Comptes Rendues Geoscience, **329**: 317–323.

Choubert, G., and Hupé, P. 1953. Formations géorgiennes à trilobites sur pourtour de l'Anti-Atlas central. Comptes Rendues Geoscience, **237**: 1168–1171.

Choubert, G., Boudda, A., and Faure-Muret, A. 1975. Essai de stratigraphie de la couverture sedimentaire de l'Anti-Atlas: Adoudouniene – Cambrien inférieur: Agadir-Rabat, 57 p.

Cloud, P., and Glaessner, M. 1982. The Ediacaran period and system: Metazoa inherit the Earth. Science, **217**: 783–792.

Compston, W., Williams, I., Kirschvink, J., Zichao, Z., and Guogan, M. 1992. Zircon U–Pb ages from the Early Cambrian time-scale. Journal of the Geological Society (of London), **149**: 171–184.

Conway Morris, S. 1993. Ediacaran-like fossils in Cambrian Burgess Shale-type faunas of North America. Paleontology, **36**: 593–635.

Corsetti, F., and Hagadorn, J. 2000. Precambrian-Cambrian transition: Death Valley, United States. Geology, **28**(4): 299–302.

Cramer, B., and Saltzman, M. 2005. Sequestration of ^{12}C in the deep ocean during the early Wenlock (silurian) positive carbon isotope excursion. Palaeogeography, Palaeoclimatology, Palaeoecology, **219**: 333–349.

Crimes, T. 1987. Trace fossils and correlation of the late Precambrian and early Cambrian strata. Geological Magazine, **124**: 97–119.

Crimes, T., and McIlroy, D. 1999. A biota of Ediacaran aspect from lower Cambrian strata on the Digermul Peninsula, Arctic Norway. Geological Magazine, **136**(6): 633–642.

Crimes, T., Insole, A., and Williams, B. 1995. A rigid-bodied Ediacaran Biota from Upper Cambrian Strata in Co. Wexford, Eire. Geological Journal, **30**: 89–109.

Debrenne, F. 1991. Extinction of the Archaeocyathia. Historical Biology, **5**: 95–106.

Debrenne, F., and Debrenne, M. 1978. Archaeocyathid fauna of the lowest fossiliferous levels of Tiout (Lower Cambrian - Southern Morocco). Geological Magazine, **115**: 101–120.

Debrenne, F., and Debrenne, M. 1995. Archaeocyaths of the Lower Cambrian of Morocco. *In* Morocco '95: The Lower-Middle Cambrian standard of Western Gondwana. Beringeria, Würtzburg, Vol. 28, pp. 121–145.

Des Marais, D. 1997. Long-term evolution of the biogeochemical carbon cycle. *In* Geomicrobiology: interactions between microbes and minerals. *Edited by* J. Banfield and K. Nealson. Mineralogical Society of America, Washington, D.C., Vol. 357, pp. 429–448.

Destombes, J., Hollard, H., and Willefert, S. 1985. Lower Palaeozoic Rocks of Morocco. *In* Lower Palaeozoic of north-western and west central Africa. *Edited by* C. Holland. Lower Palaeozoic Rocks of the World. Vol. 4, John Wiley & Sons, New York, N.Y., pp. 91–336.

Dickens, G. 2003. Rethinking the global carbon cycle with a large, dynamic and microbially mediated gas hydrate capacitor. Earth and Planetary Science Letters, **213**: 169–183.

Dickens, G., O'Neil, J., Rea, D., and Owen, R. 1995. Dissociation of oceanic methane hydrate as a cause of the carbon isotope excursion at the end of the Paleocene. Paleoceanography, **10**(6): 965–971.

Droser, M., Gehling, J., and Jensen, S. 1999. When the worm turned; concordance of Early Cambrian ichnofabric and trace-fossil record in siliciclastic rocks of South Australia. Geology, **27**(7): 625–628.

Droser, M., Jensen, S., and Gehling, J. 2002. Trace fossils and substrates of the terminal Proterozoic-Cambrian transition: Implications for the record of early bilaterians and sediment mixing. Proceedings of the National Academy of Sciences, **99**(20): 12 572 – 12 576.

Ducrot, J. 1979. Datation à 615 Ma de la granodiorite de Bleida et conséquences sur la chronolgie des phases tectoniques, métamorphiques et magmatiques pan-africaines dans l'Anti-Atlas marocain. Bulletin de la Societé géologique Français, **4**: 495–499.

Ducrot, J., and Lancelot, J. 1977. Problème de la limite Précambrien–Cambrien: étude radiochronogique par la méthode U/Pb sur zircons du volcan du Jbel Boho. Canadian Journal of Earth Science, **14**: 2771–2777.

El Aouli, E., Gasquet, D., and Ikenne, M. 2001. Le magmatisme basique de la boutonnière d'Igherm (Anti-Atlas occidental, Maroc): un jalon des distension néoprotérozoïques sur la bordure nord du craton ouest-africain. Bulletin de la Societé géologique Français, **172**(3): 309–317.

El Boukhari, A., Chabane, A., Rocci, G., and Tane, J.-L. 1992. Upper Proterozoic ophiolites of the Siroua Massif (Anti-Atlas, Morocco) a marginal sea and transform fault system. Journal of African Earth Sciences, **14**(1): 67–80.

Faik, F., Belfoul, M., Bouabdelli, M., and Hassenforder, B. 2001. Les structures de la couverture Néoproterozoïque terminal et Paléozoïque de la région de Tata, Anti-Atlas centre-occidental, Maroc: déformation polyphasée, ou interactions socle/couverture pendant l'orogenèse hercynienne? Journal of African Earth Sciences, **32**(4): 765–776.

Fedonkin, M. 1990. Systematic descriptions of Vendian Metazoa. *In* The Vendian System, Vol. 1. *Edited by* B. Sokolov and A. Iwanoski. Springer, Heidelberg, Germany, pp. 71–120.

Fekkak, A., Boualoul, M., Badra, L., Amenzou, M., Saquaque, A., and El-Amrani, I. 2000. Origine et contexte geotectonique des depots detritiques du Groupe Neoproterozoïque inferieur de Kelaat Mgouna (Anti-Atlas Oriental, Maroc). Journal of African Earth Sciences, **30**(2): 295–311.

Fekkak, A., Pouclet, A., Ouguir, H., Ouazzani, H., and Badra, L. 2001. Géochimie et signification géotectonique des volcanites du Cryogénien inférieur de Saghro (Anti-Atlas oriental, Maroc). Geodinamica Acta, **14**: 373–385.

Fekkak, A., Pouclet, A., and Badra, L. 2002. The Pre-Pan-African rifting of Saghro (Anti-Atlas, Morocco): example of the middle Neoproterozoic Basin of Boumalne. Bulletin de la Societé géologique Français, **173**(1): 25–35.

Frizon de Lamotte, D., Saint Bezar, B., Bracène, R., and Mercier, E. 2000. The two main steps of the Atlas building and geodynamics of the western Mediterranean. Tectonics, **19**(4): 740–761.

Gehling, J., Jensen, S., Droser, M., Myrow, P., and Narbonne, G. 2001. Burrowing below the basal Cambrian GSSP, Fortune Head, Newfoundland. Geological Magazine, **138**(2): 213–218.

Germs, G. 1972. New shelly fossils from the Nama Group, South-West Africa. American Journal of Science, **272**: 752–761.

Gerstenberger, H., and Haase, G. 1997. A highly effective emitter substance for mass spectrometric Pb isotope ratio determinations. Chemical Geology, **136**: 309–312.

Geyer, G. 1989. Late Precambrian to early Middle Cambrian lithostratigraphy of southern Morocco. Beringeria, **1**: 115–143.

Geyer, G., and Landing, E. 1995. The Cambrian of the Moroccan Atlas regions. *In* Morocco '95: The Lower-Middle Cambrian standard of Western Gondwana. Beringeria, Würtzburg, Vol. 28, pp. 7–46.

Goldhammer, R., Dunn, P., and Hardie, L. 1987. High frequency glacio-eustatic sealevel oscillations with Milankovitch characteristics recorded in Middle Triassic platform carbonates in Northern Italy. American Journal of Science, **287**: 853–892.

Gomez, F., Beauchamp, W., and Barazangi, M. 2000. Role of the Atlas Mountains (northwest Africa) within the African–Eurasian plate-boundary zone. Geology, **28**(9): 775–778.

Goodwin, P., and Anderson, E. 1985. Puncuated aggradational cycles: A general hypothesis of episodic stratigraphic accumulation. Journal of Geology, **93**: 515–533.

Grant, S. 1990. Shell structure and distribution of *Cloudina*, a potential index fossil for the terminal Proterozoic. American Journal of Science, **290-A**: 261–294.

Gregory, R., and Taylor, H. 1981. An oxygen isotope profile in a section of Cretaceous oceanic crust, Samail ophiolite, Oman; evidence for a $\delta^{18}O$ buffering of the oceans by deep (>5 km) seawater-hydrothermal circulation at mid-ocean ridges. Journal of Geophysical Research, **86B**(4): 2737–2755.

Grotzinger, J. 1986. Cyclicity and paleoenvironmental dynamics, rocknest platform, northwest Canada. Geological Society of America Bulletin, **97**: 1208–1231.

Grotzinger, J., and Knoll, A. 1995. Anomalous carbonate precipitates: is the Precambrian the key to the Permian? Palaios, **100**: 578–596.

Grotzinger, J., Bowring, S., Saylor, B., and Kaufman, A. 1995. Biostratigraphic and geochronologic constraints on early animal evolution. Science, **270**: 598–604.

Grotzinger, J., Watters, W., and Knoll, A. 2000. Calcified metazoans in thrombolite-stromatolite reefs of the terminal Proterozoioc Nama Group, Namibia. Paleobiology, **26**: 334–359.

Hafid, A., Sagon, J., Julivert, M., Arboleya, M., Saquaque, A., El-Boukhari, A., Saidi, A., and Soler, J. 2001. Le magmatisme basique filonien néoproterozoïque de la boutonnière de Zenaga, Anti-Atlas central, Maroc: pétrologie, géochimie et signification géodynamique. Journal of African Earth Sciences, **32**(4): 707–721.

Hagadorn, J., Fedo, C., and Waggoner, B. 2000. Early Cambrian Ediacran-type fossils from California. Journal of Paleontology, **74**(4): 731–740.

Hambrey, M., and Harland, W. 1981. Earth's Pre-Pleistocene Glacial Record. Cambridge University Press, London, UK.

Hassenforder, B., Roger, J., Baudin, T., Chalot-Prat, F., Gasquet, D., Berrahma, A., Chèvremont, P., Marquer, D., Razin, P., and Benlakhdim, A. 2001. Carte géologique au 1/50000 feuille Sidi Bou'Addi. Notes et Mémoires du Service Géologique, **414**.

Hayes, J., Strauss, H., and Kaufman, A. 2001. Fractionation of the isotopes of carbon and hydrogen in biosynthetic processes. *In* GSA Short course sponsored by the Mineralogical Society of America. *Edited by* J. Valley and D. Cole. pp. 1–31.

Hedges, J., and Keil, R. 1995. Sedimentary organic-matter preservation—An assessment and speculative synthesis. Marine Chemistry, **49**: 81–115.

Hefferan, K., Karson, J., and Saquaque, A. 1992. Proterozoic collisional basins in a Pan-African suture zone, Anti-Atlas Mountains, Morocco. Precambrian Research, **54**: 295–319.

Hefferan, K., Admou, H., Karson, J., and Saquaque, A. 2000. Anti-Atlas (Morocco) role in Neoproterozoic Western Gondwana reconstruction. Precambrian Research, **103**: 89–96.

Hoffmann, H., and Mountjoy, E. 2001. *Namacalathus–Cloudina* assemblage in Neoproterozoic Miette Group (Byng Formation), British Columbia: Canada's oldest shelly fossils. Geology, **29**: 1091–1094.

Holmden, C., and Muehlenbachs, K. 1993. The $^{18}O/^{16}O$ ratio of 2-billion year-old seawater inferred from ancient oceanic crust. Science, **259**(5102): 1733–1736.

Holser, W., Schidlowski, M., Mackenzie, F., and Maynard, J. 1988. Geochemical cycles of carbon and sulfur. *In* Chemical cycles in the evolution of the Earth. *Edited by* C. Gregory, R. Garrels, F. Mackenzie, and J. Maynard. Wiley, John & Sons, New York, pp. 105–173.

Houzay, J.-P. 1979. Empreintes attribuables à des méduses dans la série de base de lÁdoudounien (Précambrien terminal de l'Anti-Atlas, Maroc). Géologie Méditerranéenne, **3**: 379–384.

Hupé, P. 1953. Contribution à l'étude du Cambrien inférieur et du Précambrien III de l'Anti-Atlas marocain. Notes et Mémoires du Service Géologique du Maroc, **103**: 402.

Hurley, P., Boudda, A., Kanes, W., and Nairn, A. 1974. A plate tectonics origin for Late Precambrian–Paleozoic orogenic belt in Morocco. Geology, **2**(7): 343–344.

Ingall, E., and Jahnke, R. 1997. Influence of water-column anoxia on the elemental fractionation of carbon and phosphorous during sediment diagenesis. Marine Geology, **139**: 219–229.

Ingall, E., and VanCappellen, P. 1990. Relation between sedimentation rate and burial of organic phosphorous and organic carbon in marine sediments. Geochimica Cosmochimicha Acta, **54**: 373–386.

Ingall, E., Bustin, R., and VanCappellen, P. 1993. Influence of water-column anoxia on the burial and preservation of carbon and phosphorous in marine shales. Geochimica Cosmochimicha Acta, **57**: 303–316.

Inglis, J., MacLean, J., Samson, S., D'Lemos, R., Admou, H., and Hefferan, K. 2004. A precise U-Pb zircon age for the Bleida granodiorite, Anti-Atlas, morocco: implications for the timing of deformation and terrane assembly in the eastern Anti-Atlas. Journal of African Earth Sciences, **39**: 277–283.

Isachsen, C., Bowring, S., Landing, E., and Samson, S. 1994. New constraint on the division of Cambrian time. Geology, **22**: 496–498.

Jacobsen, S., and Kaufman, A. 1999. The Sr, C, and O isotopic evolution of Neoproterozoic seawater. Chemical Geology, **161**: 37–57.

Jaffey, A., Flynn, K., Glendenin, L., Bentley, W., and Essling, A. 1971. Precision measurement of half-lives and specific activities of ^{235}U and ^{238}U. Physical Review, **C4**: 1889–1906.

Jensen, S., Gehling, J., and Droser, M. 1998. Ediacara-type fossils in Cambrian sediments. Nature, **393**: 567–569.

Jensen, S., Saylor, B., Gehling, J., and Germs, G. 2000. Complex trace fossils from the terminal Proterozoic of Namibia. Geology, **28**(2): 143–146.

Junge, C., Schidlowski, M., Eichmann, R., and Pietrek, H. 1975. Model calculations for the terrestrial carbon cycle: Carbon isotope geochemistry and evolution of photosynthetic oxygen. Journal of Geophysical Research, **80**(B): 4542–4552.

Kaufman, A., Knoll, A., Semikhatov, M., Grotzinger, J., Jacobsen, S., and Adams, W. 1996. Integrated chronostratigraphy of Proterozoic–Cambrian boundary beds in the western Anabar region, northern Siberia. Geological Magazine, **133**(5): 509–533.

Kaufman, A., Knoll, A., and Narbonne, G. 1997. Isotopes, ice ages, and terminal Proterozoic Earth history. Proceedings of the National Academy of Sciences, **95**: 6600–6605.

Keil, R., con, D.M., Prahl, F., and Hedges, J. 1994. Sorptive preservation of labile organic matter in marine sediments. Nature, **370**: 549–552.

Kendall, C., and Warren, J. 1987. A review of the origin and setting of teepees and their associated fabrics. Sedimentology, **34**: 1007–1028.

Kennedy, M., Pevear, D., and Hill, R. 2002. Mineral surface control on organic carbon in black shale. Science, **295**(5555): 654–657.

Khomentovsky, V., and Karlova, G. 1993. Biostratigraphy of the Vendian–Cambrian beds and the lower Cambrian boundary in Siberia. Geological Magazine, **130**: 29–45.

Kimura, H., and Watanabe, Y. 2001. Ocean anoxia at the Precambrian–Cambrian boundary. Geology, **29**(11): 995–998.

Kirschvink, J., Magaritz, M., Ripperdan, R., Zhuravlev, A., and Rosanov, A. 1991. The Precambrian/Cambrian boundary: Magnetostratigraphy and carbon isotopes resolve correlation problems between Siberia, Morocco, and South China. GSA Today, **1**: 69–71,87,91.

Knoll, A., and Carroll, S. 1999. Early animal evolution: Emerging views from comparative biology and geology. Science, **284**: 2129–2137.

Knoll, A., Grotzinger, J., Kaufman, A., and Kolosov, P. 1995*a*. Integrated approaches to terminal Proterozoic stratigraphy: an example from the Olenek Uplift, northeastern Siberia. Precambrian Research, **73**: 251–270.

Knoll, A., Kaufman, A., Semikhatov, M., Grotzinger, J., and Adams, W. 1995*b*. Sizing up the sub-Tommotian unconformity in Siberia. Geology, **23**(12): 1139–1143.

Kominz, M., and Bond, G. 1990. A new method of testing periodicity in cyclic sediments: application to the Newark Supergroup. Earth and Planetary Science Letters, **98**: 233–244.

Kooi, H., and Cloetingh, S. 1992. Lithospheric necking and regional isostasy at extensional basins 2. Stress-induced vertical motions and relative sea level changes. Journal of Geophysical Research, **97**(B12): 17 573 – 17 591.

Kooi, H., Cloetingh, S., and Burrus, J. 1992. Lithospheric necking and regional isostasy at extensional basins 1. Subsidence and gravity modeling with an application to the Gulf of Lions Margin (SE France). Journal of Geophysical Research, **97**(B12): 17 533 – 17 571.

Kouchinsky, A., Bengston, S., Missarzhevsky, V., Pelechaty, S., Torssander, P., and Val'kov, A. 2001. Carbon isotope stratigraphy and the problem of a pre-Tommotian Stage in Siberia. Geological Magazine, **138**(4): 387–396.

Krogh, T. 1973. A low contamination method for the hydrothermal decomposition of zircon and extraction of U and Pb for isotopic age determinations. Geochimica Cosmochimicha Acta, **37**: 485–494.

Krogh, T. 1982. Improved accuracy of U–Pb zircon ages by creation of more concordant systems using an air abrasion technique. Geochimica Cosmochimicha Acta, **145**: 637–649.

Kump, L. 1991. Interpreting carbon-isotopic excursions: Strangelove oceans. Geology, **1991**: 299–302.

Kump, L. 1993. The coupling of the carbon and sulfur biogeochemical cycles over Phanerozoic time. *In* Interactions of C, N, P and S biogeochemical cycles and global change. *Edited by* R. Wollast, F. Mackenzie, and L. Chou. NATO ASI Series I: Global Environmental Change, Springer-Verlag, Berlin, Germany, Vol. 4, pp. 475–490.

Kump, L.R. 1988. Terrestrial feedback in atmospheric oxygen regulation by fire and phosphorus. Nature, **335**: 152–154.

Kump, L., Arthur, M., Patzkowsky, M., Gibbs, M., Pinkus, D., and Sheehan, P. 1999. A weathering hypothesis for glaciation at high atmospheric pCO_2 during the Late Ordovician. Palaeogeography, Palaeoclimatology, Palaeoecology, **152**: 173–187.

Landing, E., Bowring, S., Davidek, K., Westrop, S., Geyer, G., and Heldmaier, W. 1998. Duration of the Early Cambrian: U–Pb ages of volcanic ashes from Avalon and Gondwana. Canadian Journal of Earth Science, **35**: 329–338.

Latham, A., and Riding, R. 1990. Fossil evidence for the location of the Precambrian/cambrian boundary in Morocco. Nature, **344**: 752–754.

Leblanc, M. 1976. Proterozoic oceanic crust at Bou Azzer. Nature, **261**: 34–35.

Leblanc, M., and Lancelot, J. 1972. Sur le style disharmonique des plis hercyniens à la base de la couverture, dans l'Anti-Atlas central (Maroc). Comptes Rendues Geoscience, **275**(D): 803–807.

Lenton, T., and Watson, A. 2000. Redfield revisited: 1. Regulation of nitrate, phosphate, and oxygen in the ocean. Global Biogeochemical Cycles, **14**(1): 225–248.

Long, D. 1993. Oxygen and carbon isotopes and event stratigraphy near the Ordovician-Silurian boundary, Anticosti Island Quebec. Palaeogeography, Palaeoclimatology, Palaeoecology, **104**: 49–59.

Ludwig, K. 1980. Calculation of uncertainties of U–Pb isotope data. Earth and Planetary Science Letters, **46**: 212–220.

Ludwig, K. 1991. Isoplot-a plotting and regression program for radiogenic isotope data. Technical report, US Geological Survey.

Ludwig, K. 1998. On the treatment of concordant uranium–lead ages. Geochimica Cosmochimicha Acta, **62**: 665–676.

Magaritz, M. 1989. ^{13}C minima follow extinction events: A clue to faunal radiation. Geology, **17**: 337–340.

Magaritz, M., Latham, A., and Kirschvink, J. 1986. Carbon isotope events across the Precambrian/Cambrian boundary on the Siberian Platform. Nature, **320**: 258–259.

Magaritz, M., Kirschvink, J., Latham, A., Zhuralev, A., and Rozanov, A. 1991. Precambrian/Cambrian boundary problem: Carbon isotope correlations for Vendian and Tommotian time between Siberia and Morocco. Geology, **19**: 847–850.

Maloof, A. 2004. Thermal contraction cracks, polar wandering, and global carbon cycling: non-uniformitarian changes that shaped the Neoproterozoic and Early Cambrian Earth. Ph.D. thesis, Harvard University, Cambridge, Mass.

Marshall, J., Brenchley, P., Mason, P., Wolff, G., Astini, R., Hints, L., and Meidla, T. 1997. Global carbon isotopic events associated with mass extinctions and glaciation in the late Ordovician. Palaeogeography, Palaeoclimatology, Palaeoecology, **132**: 195–210.

Martin, M., Grazhdankin, D., Bowring, S., Evans, D., Fedonkin, M., and Kirschvink, J. 2000. Age of Neoproterozoic bilaterian body and trace fossils, White Sea, Russia: Implications for Metazoan Evolution. Science, **288**: 841–845.

Mattinson, J. 2000. Revisiting the "gold standard" — the uranium decay constants of Jaffey et al., 1971. Eos Transactions of the American Geophysical Union, Spring Meeting Supplement, Abstract V61A-02.

Mattinson, J. 2003. CA (chemical abrasion) – TIMS: high-resolution U–Pb zircon geochronology combining high-temperature annealing of radiation damage and multi-step partial dissolution analysis. Eos Transactions of the American Geophysical Union, Fall Meeting Supplement, Abstract V22E-06.

Mayer, L. 1999. Extent of coverage of mineral surfaces by organic matter in marine sediments. Geochimica Cosmochimicha Acta, **63**: 207–215.

Michard, A. 1976. Eléments de Géologie Marocaine. Notes et Mémoires du Service Géologique du Maroc, **252**: 368.

Mifdal, A., and Peucat, J.-J. 1985. Datations U–Pb et Rb–Sr du volcanisme acide de l'Anti-Atlas Marocain et du socle sous-jacent dans la région de Ouarzazate apport au problème de la limite Précambrien-Cambrien. Sci. Géol. Bull. **38**(2): 185–200.

Monninger, W. 1979. The section of Tiout (Precambrian/Cambrian boundary beds, Anti-Atlas, Morocco): An environmental model. Arb. Paläont. Inst., Würtzburg, **1**: 289–302.

Mortaji, A., Ikenne, M., Gasquet, D., Barbey, P., and Stussi, J. 2000. Les granitoïdes paléoprotérozoïques des boutonnières du bas drâa and Tagragra d'Akka Inliers (Anti-Atlas occidental, Maroc): un élément du puzzle géodynamique du craton ouest-africain. Journal of African Earth Sciences, **31**: 523–538.

Muehlenbachs, K. 1998. The oxygen isotopic composition of the oceans, sediments and the seafloor. Chemical Geology, **145**(3–4): 263–273.

Muehlenbachs, K., and Clayton, R. 1976. Oxygen isotopic composition of the oceanic crust and its bearing on seawater. Journal of Geophysical Research, **81**(23): 4365–4369.

Narbonne, G. 1998. The Ediacara biota: A terminal Neoproterozoic experiment in the evolution of life. GSA Today, **8**(2): 1–6.

Narbonne, G., and Gehling, J. 2003. Life after snowball: The oldest complex Ediacaran fossils. Geology, **31**: 27–30.

Narbonne, G., Kaufman, A., and Knoll, A. 1994. Integrated chemostratigraphy and biostratigraphy of the Windermere Supergroup, northwestern Canada; implications for Neoproterozoic correlations and the early evolution of animals. Geological Society of America Bulletin, **106**(10): 1281–1292.

Orr, P., Benton, M., and Briggs, D. 2003. Post-Cambrian closure of the deep-water slope-basin taphonomic window. Geology, **31**(9): 769–772.

Ouguir, H., Macaudière, J., and Dagallier, G. 1996. Le Protérozoïque supérieur dImiter, Saghro oriental, Maroc: un contexte géodynamique d'arrière-arc. Journal of African Earth Sciences, **22**(2): 173–189.

Payne, J., Lehrmann, D., Wei, J., Orchard, M., Schrag, D., and Knoll, A. 2004. Large perturbations of the carbon cycle during recovery from the End-Permian extinction. Science, **305**: 506–509.

Pearson, P., Ditchfield, P., Singano, J., Harcourt-Brown, K., Nicholas, C., Olsson, R., Shackleton, N., and Hall, M. 2001. Warm tropical sea surface temperatures in the Late Cretaceous. Nature, **413**: 481–487.

Pelechaty, S., Grotzinger, J., Kashirtsev, V., and Zhernovsky, V. 1996. Chemostratigraphic and sequence stratigraphic constraints on Vendian–Cambrian basin dynamics, Northeast Siberian craton. Journal of Geology, **104**: 543–563.

Piqué, A. 2003. Evidence for an important extensional event during the latest proterozoic and earliest paleozoic in morocco. Comptes Rendues Geoscience, **335**: 865–868.

Piqué, A., Bouabdelli, M., Soulaïmani, A., Youbi, N., and Iliani, M. 1999. Les congomlérats de PIII (Néoprotérozoïque supérieur) de l'Anti-Atlas (Sud du Maroc): molasses panafricaines, ou marqueurs d'un rifting fini-protérozoïques? Comptes Rendues Geoscience, **328**: 409–414.

Porter, S. 2004. Closing the Phosphatization window: testing for the influence of taphonomic megabias on the pattern of small shelly fossil decline. Palaios, **19**: 178–183.

Roger, J., Gasquet, D., Baudin, T., Chalot-Prat, F., Hassenforder, B., Marquer, D., Chèvremont, P., Berrahma, A., Destombes, J., Razin, P., and Benlakhdim, A. 2001. Carte géologique au 1/50000 feuille Tamazrar. Notes et Mémoires du Service Géologique du Maroc, **415**.

Rothman, D., Hayes, J., and Summons, R. 2003. Dynamics of the Neoproterozoic carbon cycle. Proceedings of the National Academy of Sciences, **100**(14): 124–129.

Rowland, S., Luchinina, V., Korovnikov, I., Sipin, D., Tarletskov, A., and Fedoseev, A. 1998. Biostratigraphy of the Vendian–Cambrian Sukharikha River section, northwestern Siberian Platform. Canadian Journal of Earth Science, **35**: 339–352.

Saadi, S., Hilali, E., Bensaïd, M., Boudda, A., and Dahmani, M. 1985. Carte Géologique de Maroc. Ministère de l'Énergie et des Mines, Direction de la Géologie, Rabat.

Saltzman, M. 2001. Silurian δ^{13}C stratigraphy: a view from North America. Geology, **29**(8): 671–674.

Saltzman, M. 2002. Carbon isotope (δ^{13}C) stratigraphy acros the Silurian–Devonian transition in North America: evidence for a perturbation of the global carbon cycle. Palaeogeography, Palaeoclimatology, Palaeoecology, **187**: 83–100.

Saltzman, M., and Young, S. 2005. Long-lived glaciation in the Late Ordovician? Isotopic and sequence-stratigraphic evidence from western Laurentia. Geology, **33**(2): 109–112.

Saltzman, M.R. 2005. Phosphorous, nitrogen, and the redox evolution of the Paleozoic oceans. Geology, **33**(7): 573–576.

Samson, S., and D'Lemos, R. 1998. U–Pb geochronology and Sm–Nd isotopic composition of Proterozoic gneisses, Channel Islands, UK. Journal of the Geological Society (of London), **155**: 609–618.

Samson, S., Inglis, J., D'Lemos, R., Admou, H., Blichert-Toft, J., and Hefferan, K. 2004. Geochronological , geochemical, and Nd–Hf isotopic constraints on the origin of Neoproterozoic plagiogranites in the Tasriwine ophiolite, Anti-Atlas orogen, Morocco. Precambrian Research, **135**: 133–147.

Saquaque, A., Admou, H., Karson, J., Hefferan, K., and Reuber, I. 1989. Precambrian accretionary tectonics in the Bou Azzer-El Graara region, Anti-Atlas, Morocco. Geology, **17**: 1107–1110.

Schrag, D., Berner, R., Hoffman, P., and Halverson, G. 2002. On the initiation of a snowball Earth. Geochemistry, Geophysics, and Geosystems, **300**: p. 10.1029/2001GC000,219.

Seilacher, A. 1984. Late Precambrian and Early Cambrian metazoa: Preservational or real extinctions? *In* Patterns of change in Earth evolution. *Edited by* H. Holland and A. Trendall. Springer-Verlag, Berlin, Germany, pp. 159–168.

Smith, S. 1984. Phosphorous versus nitrogen limitation in the marine environment. Limnology Oceanography, **29**: 1149–1160.

Soulaïmani, A., Piqué, A., and Bouabdelli, M. 2001. La série du PII-III de l'Anti-Atlas occidental (Sud marocain): un olistostrome à la base de la couverture post-panafricaine (PIII) du Protérozoïque supérieur. Comptes Rendues Geoscience, **332**: 121–127.

Soulaïmani, A., Bouabdelli, M., and Piqué, A. 2003. L'extension continentale au Néo-Protérozoïque supérieur-Cambrien inférieur dans l'Anti-Atlas (Maroc). Bulletin de la Societé géologique Français, **174**(1): 83–92.

Spero, H., Bijma, J., Lea, D., and Bemis, B. 1997. Effect of seawater carbonate concentration on foraminiferal carbon and oxygen isotopes. Nature, **390**(6659): 497–500.

Thomas, R., Chevallier, L., Gresse, P., Harmer, R., Eglington, B., Armstrong, R., de Beer, C., Martini, J., de Kock, G., Macey, P., and Ingram, B. 2002. Precambrian evolution of the Sirwa Window, Anti-Atlas Orogen, Morocco. Precambrian Research, **118**: 1–57.

Tucker, M. 1986. Carbon isotope excursions in Precambrian/Cambrian boundary beds, Morocco. Nature, **319**: 48–49.

Tyrrell, T. 1999. The relative influences of nitrogen and phosphorous on oceanic primary production. Nature, **400**: 525–531.

VanCappellen, P., and Ingall, E. 1996. Redox stabilization of the atmosphere and oceans by phosphorous-limited marine productivity. Science, **271**: 493–496.

Veizer, J., Ala, D., Azmy, K., Bruckschen, P., Buhl, D., Bruhn, F., Carden, G., Diener, A., Ebneth, S., Godderis, Y., Jasper, T., Korte, C., Pawellek, F., Podlaha, O., and Strauss, H. 1999. ^{87}Sr/^{86}Sr, δ^{13}C and δ^{18}O evolution of Phanerozoic seawater. Chemical Geology, **161**: 59–88.

Walsh, G., Aleinikoff, J., Benziane, F., Yazidi, A., and Armstrong, T. 2002. U–Pb zircon geochronology of the Paleoproterozoic Tagrara de Tata inlier and its Neoproterozoic cover, western Anti-Atlas, Morocco. Precambrian Research, **117**: 1–20.

Watters, W., and Grotzinger, J. 2001. Digital reconstruction of calcified early metazoans, terminal Proterozoic Nama Group, Namibia. Paleobiology, **27**: 159–171.

Wilkinson, B., Drummond, C., Rothman, E., and Diedrich, N. 1997. Stratal order in peritidal carbonate sequences. Journal of Sedimentary Research, **67**(6): 1068–1082.

Wilkinson, B., Drummond, C., Diedrich, N., and Rothman, E. 1999. Poisson processes of carbonate accumulation on Paleozoic and Holocene platforms. Journal of Sedimentary Research, **69**(2): 338–350.

Wood, R., Grotzinger, J., and Dickson, J. 2002. Proterozoic modular biomineralized metazoan from the Nama Group, Namibia. Science, **296**: 2383–2386.

Yang, W., Harmsen, F., and Kominz, M. 1995. Quantitative analysis of a cyclic peritidal carbonate sequence, the Middle and Upper Devonian

Lost Burro Formation, Death Valley, California—A possible record of Milankovitch climatic cycles. Journal of Sedimentary Research, **B65**(3): 306–322.

York, D. 1966. Least-squares fitting of a straight line. Canadian Journal of Physics, **44**: 1079–1086.

York, D. 1967. The best isochron. Earth and Planetary Science Letters, **2**: 479–482.

Zachos, J., Wara, M., Bohaty, S., Delaney, M., Petrizzo, M., Brill, A., Bralower, T., and Premoli-Silva, I. 2003. A transient rise in tropical sea surface temperature during the Paleocene–Eocene thermal maximum. Science, **302**: 1551–1554.

Zachos, J., Roehl, U., Hodell, D., Thomas, E., Sluijs, S., Schellenberg, S., Kelly, C., McCarren, H., Kroon, D., and Nicolo, M. 2004. Extreme acidification of the deep sea at the Paleocene-Eocene boundary: New constraints from Ocean Drilling Program Leg 208. *In* EOS transactions of American Geophysical Union Fall Meeting, San Francisco, Calif., Abstracts, p. B561.

Zhuravlev, A. 1986. Evolution of archaeocyaths and palaeobiogeography of the Early Cambrian. Geological Magazine, **123**(4): 377–386.

Zuber, M., and Parmentier, E. 1986. Lithospheric necking: a dynamic model for rift morphology. Earth and Planetary Science Letters, **77**: 373–383.